NASA TM X-450

TECHNICAL MEMORANDUM

X-450

INVESTIGATION OF THE LOW SUBSONIC STABILITY AND CONTROL CHARACTERISTICS OF A HYPERSONIC BOOST-GLIDE TYPE AIRPLANE WITH WING, FUSELAGE, AND VERTICAL-TAIL MODIFICATIONS

By Robert E. Shanks

Langley Research Center
Langley Field, Va.

NATIONAL AERONAUTICS AND SPACE ADMINISTRATION

WASHINGTON

March 1961

CONFIDENTIAL

iP

[redacted]

NATIONAL AERONAUTICS AND SPACE ADMINISTRATION

TECHNICAL MEMORANDUM X-450

INVESTIGATION OF THE LOW SUBSONIC STABILITY AND CONTROL CHARACTERISTICS OF A HYPERSONIC BOOST-GLIDE TYPE AIRPLANE WITH WING, FUSELAGE, AND VERTICAL-TAIL MODIFICATIONS*

By Robert E. Shanks

SUMMARY

A static force-test investigation has been made to determine the low subsonic stability and control characteristics of several configurations of a hypersonic boost-glide vehicle having a fuselage and wing-tip vertical tails on the upper surface of the wing. In general, it was found that the vertical tails were longitudinally destabilizing, that the directional stability was increased by toeing in the vertical tails and that the lift-drag ratio was increased by boattailing the fuselage. The lateral and longitudinal controls remained effective over the angle-of-attack range but the effectiveness decreased appreciably at the angles of attack between 20° and 30°. The presence of a fuselage on the forward upper surface of the wing caused a break in the lift curve at an angle of attack of about 25° and a reduction in maximum lift coefficient.

INTRODUCTION

An investigation is being conducted by the National Aeronautics and Space Administration to provide information on some proposed hypersonic boost-glide configurations over the speed range from hypersonic to low subsonic speeds. Some of the results at transonic and supersonic speeds are reported in references 1 to 3. The present investigation was made to provide some information at low subsonic speeds on the longitudinal and lateral stability characteristics of some of the hypersonic boost-glide airplane configurations reported in reference 4 with various geometric modifications. The configurations tested included one clipped-delta and several cranked, clipped-delta planforms with the fuselage and

*Title, Unclassified.

[redacted]

the wing tip vertical tails on the upper surface of the wing. The large number of modifications considered is a result of various exploratory tests made in an effort to provide some information on means of improving the stability characteristics and lift-drag ratios.

Most of the investigation was made over a range of angles of attack from 0° to 30°; a few tests were made up to an angle of attack of 90°. Tests were made to determine the effect of trailing-edge wing-chord extensions, fuselage boattail modifications, and vertical-tail geometry and toe angle on the longitudinal and lateral stability and control characteristics of the models.

SYMBOLS

The lateral data are referred to the body system of axes (fig. 1) and the longitudinal data are referred to the wind system of axes. The origin of the axes was located at a longitudinal center-of-gravity position of 64-percent body length except as noted. (For corresponding percent of mean aerodynamic chords, see table I.) All coefficients are based on individual areas and mean aerodynamic chords.

b wing span, ft

$\bar{c}$ wing mean aerodynamic chord, ft

C_D drag coefficient, F_D/qS

C_L lift coefficient, F_L/qS

C_l rolling-moment coefficient, M_X/qSb

$C_{l_\beta} = \frac{\partial C_l}{\partial \beta}$ per degree

C_m pitching-moment coefficient, $M_Y/qS\bar{c}$

C_{m_o} pitching-moment coefficient at $C_L = 0$

C_n yawing-moment coefficient, M_Z/qSb

$C_{n_\beta} = \frac{\partial C_n}{\partial \beta}$ per degree

C_Y side-force coefficient, F_Y/qSb

$C_{Y_\beta} = \frac{\partial C_Y}{\partial \beta}$ per degree

D drag, lb

F_D drag force, lb

F_L lift force, lb

F_Y side force, lb

i_v vertical-tail toe angle (angle between the planes of symmetry of the vertical tail and the model), positive when toed-in and negative when toed-out, deg

L lift, lb

l fuselage length, in.

M_X rolling moment, ft-lb

M_Y pitching moment, ft-lb

M_Z yawing moment, ft-lb

q dynamic pressure, $\rho V^2/2$, lb/sq ft

R radius, in.

S wing area, sq ft

V airspeed, ft/sec

x,y,z coordinate axes

α angle of attack, deg

β angle of sideslip, deg

δ_a differential elevon deflection as ailerons, $\delta_{eR} - \delta_{eL}$, deg

δ_e simultaneous elevon deflection as elevator, deg

δ_r rudder deflection, deg

ρ air density, slugs/cu ft

Subscripts:

L left

R right

APPARATUS AND MODELS

The models were tested in a low-speed tunnel with a 12-foot octagonal test section at the Langley Research Center. Each model was sting-mounted and the forces and moments were measured about the body axes by means of three-component internal strain-gage balances.

The investigation was made with 0.097-scale models of proposed airplanes; these models were constructed of aluminum alloy. Three-view drawings of the models used in the tests are shown in figures 2 to 4. The various configurations are identified by numerical subscripts to letters indicating model components, B (body), W (wing), F (wing chord-extension), and V (vertical tail). For convenience in locating the details of the particular configurations the following table is presented.

Fuselage	Figure	Wing	Figure	Wing chord-extensions	Figure	Vertical tail	Figure
B_1	2(a)	W_1	2(a)	F_1	2(b)	V_1	2(b)
B_2	3(a)	W_4	2(a)	F_2	2(b)	V_2	2(b)
B_3	3(b)	W_5	3(a)	F_3	2(b)	V_3	2(b)
B_4	3(b)	W_6	4			V_4	2(b)
B_5	3(b)					V_5	3(a)
B_6	4					V_6	3(a)
						V_7	4

The wings (including the chord-extensions F_1, F_2, and F_3) and all but two (V_5 and V_7) of the vertical tails had a 1/8-inch flat-plate airfoil section to facilitate construction. A balsa cap was added to wing W_6 for some tests to give a thicker cambered wing section considered suitable for hypersonic design. Vertical tails V_5 and V_7 had wedge and modified wedge sections as shown on figures 3(a) and 4, respectively. The toe angles of the vertical tails were changed by rotating the tails about the 50-percent root-chord point. The trailing edges of vertical tails V_1 were located at the trailing edge of wing W_1 for the longitudinal tests to compare wing-chord extensions F_1, F_2, and F_3, but for the lateral tests to compare vertical tails V_1, V_2, V_3, and V_4, the trailing edges of the vertical tails were all on the trailing edges of flaps F_2. The significant geometric characteristics of the wing and vertical-tail configurations are presented in table I.

TESTS

The static longitudinal and lateral stability characteristics of the models were determined for the most part over an angle-of-attack range of 0° to 30° but several of the longitudinal tests were made over angle-of-attack ranges of 0° to 50° and 0° to 90°. Most of the lateral characteristics were determined over a sideslip range of -20° to 20° for various angles of attack, although some tests were made through an angle-of-attack range at sideslip angles of ±5°. Elevator, aileron, and rudder effectiveness were determined for angles of attack from 0° to 30° for configuration $B_3W_5V_5$ only.

The tests were made at a dynamic pressure of 4.25 pounds per square foot which corresponds to an airspeed of 60 feet per second and a test Reynolds number of 383,000 per foot and an average Reynolds number based on the model mean aerodynamic chords of approximately 1,000,000.

RESULTS AND DISCUSSION

Longitudinal Stability and Control

Since most of the tests were made with thin flat-plate wings, it is desirable first of all to establish the effect of wing thickness on the longitudinal stability characteristics of the models. A comparison is therefore made in figure 5 of the longitudinal characteristics of

configuration $B_6W_6V_7$ with a 1/8-inch flat-plate wing and with a wing having an airfoil shape (1.13 inch maximum thickness). The data show that the flat-plate section produced smaller negative pitching moments but the static longitudinal stability $\left(dC_m/dC_L\right)$ of the two configurations was virtually the same. The difference in pitching moments and the relatively minor differences in the lift and drag curves (that is, zero-lift angle of attack, $C_{D_{min}}$, $C_{L_{max}}$) are typical camber and thickness effects. The L/D values are about the same for both configurations at angles of attack greater than 5°. Since there was no large effect due to wing thickness and since the effects of change in configuration were of primary interest in this study, it appeared that the use of thin flat-plate wings was suitable for the purpose of this investigation.

All the configurations studied were either longitudinally neutrally stable or unstable about the reference center-of-gravity position (0.64$\bar{c}$) at lower angles of attack (0° to 25°). This moment reference was selected so that the data of this report would be consistent with the data presented in reference 1 and with similar data obtained in other facilities.

Vertical tail.- The effect of vertical tails at various toe angles on the longitudinal characteristics is shown in figure 6 for configuration $B_1W_4V_1$ which had a thin flat-plate wing and tail surfaces. The data show that the tip tails were destabilizing and that toe angle had little effect on the longitudinal stability. A change from toe-in to toe-out, however, caused a positive shift in C_{m_o}.

The tail-off and zero-toe configurations gave about the same values of lift-drag ratio and these were higher than the values for either the toe-in or toe-out configurations up to an angle of attack of about 25°. The lower lift-drag ratios for the toed-tail configurations can probably be attributed to the higher drag of the tails. The toe-out configuration had the lowest L/D ratio throughout the angle-of-attack range.

Wing chord-extension.- The data of figure 7(a) show the effect of adding horizontal extensions to the wing trailing edge for the case of the center of gravity remaining at a constant position on the fuselage (0.64$\bar{c}$) whereas figure 7(b) shows the same data for constant percent $\bar{c}$ center-of-gravity locations. The data of figure 7(a) show that all the trailing-edge chord-extensions had a stabilizing effect, the two larger extensions, F_1 and F_3, being more effective than the smallest, F_2. It is interesting to note, however, that, when the four configurations are referred to the individual 0.40$\bar{c}$ locations (fig. 7(b)), the configuration without extensions $\left(B_1W_1V_1\right)$ is the least unstable.

Fuselage shape.- Shown in figure 8 is the effect of various fuselage boattail configurations on the longitudinal characteristics of model configuration W_5V_5. The static longitudinal stability was practically the same for all fuselage configurations at the lower angles of attack. The negative shift in the pitching-moment curve produced by fuselage B_3 suggests that the boattail at the back of the fuselage is acting like a flap or elevator deflected downward.

The lift-drag ratio generally increased with decreasing base area and in the case of fuselages B_2, B_4, and B_5 the variation of the lift-drag ratio with base area was linear. Fuselage B_3 had a higher lift-drag ratio than fuselage B_4 even though it had more volume for the same base area.

Fuselage location and size.- The results of some tests made to determine the cause for the break in the lift curve at angles of attack of 25° to 30° seen in figure 7(a) for configuration $B_1W_1V_1$ are given in figures 9 and 10. The effects of sliding the fuselage back along the wing (fig. 9) and of progressive removal of the conical forward portion of the fuselage (fig. 10) are shown in these figures. The results of both series of tests indicate that the forward portion of the fuselage was responsible for the lift-curve break because the break disappeared when the forward top surface of the wing was unobstructed by a fuselage. Evidently, the relatively large body interfered with the wing vortex flow as suggested in reference 3.

Elevator deflection.- The elevator effectiveness data for configuration $B_3W_5V_5$ are presented in figure 11. In general, the elevators produced a nearly constant increment of pitching moment up to an angle of attack of about 15° and then the effectiveness decreased with further increase in angle of attack.

Lateral Stability and Control

The variation of C_Y, C_n, and C_l with β for various angles of attack is shown in figure 12 for most of the configurations discussed herein. All of these tests are summarized in the form of the stability derivatives C_{Y_β}, C_{n_β}, and C_{l_β} plotted against angle of attack in subsequent figures. The values of these derivatives were obtained by taking the difference between the values of the coefficients measured at sideslip angles of 5° and -5°. Since some of the data are nonlinear, these derivatives should be used only to indicate trends and to provide approximate comparisons of the various configurations.

Vertical-tail thickness.- A comparison of the static lateral stability characteristics for wing fuselage configuration B_3W_5 with flat-plate vertical tails at two toe angles and the 8° wedge section vertical tails at zero-toe angle is made in figure 13. These data show that, in general, the zero-toe and 4° toe-in configurations agree well with the wedge vertical tails except for a small region at an angle of attack of about 20°. These results indicate that the flat-plate vertical tails provided reasonable simulation of the wedge vertical tails at zero toe angle when the flat-plate tails were also at zero toe angle or were toed-in to the angle of the outer surface of the wedge tail.

Vertical-tail toe angle.- The effects of toe angle on the lateral stability characteristics of models $B_3W_5V_5$ and $B_1W_4V_1$ are shown in figure 14. Model $B_3W_5V_5$ had 8° wedge vertical tails and model $B_1W_4V_1$ had flat-plate vertical tails. In general, toe angle had only a small effect on the lateral characteristics of configuration $B_3W_5V_5$. Over most of the angle-of-attack range the toed-in configuration had more directional stability, or less instability, than the toed-out configuration. Neither toe-in nor toe-out had much effect on the effective dihedral $\left(-C_{l_\beta}\right)$. The comparison is also made in figure 14(a) of the flat-plate vertical tail V_1 toed in 10° to represent the outer surface of wedge vertical tail V_5 when the tail is toed in 6°. Although the agreement for these two configurations is not quite as good as that shown in figure 13 for the case of the wedge tail at zero-toe angle, it appears that the flat-plate tail does provide satisfactory simulation of the wedge tail at the larger angles of toe-in.

Toeing the vertical tails in 10° on model $B_1W_4V_1$ (fig. 14(b)) produced small to fairly large increases in the directional stability, up to an angle of attack of about 25° but had very little effect on the dihedral parameter $-C_{l_\beta}$.

Symmetrical rudder deflection.- Use of simultaneous outward deflection of the rudders has been suggested as a means of improving the directional stability at hypersonic speeds. A few tests were made to determine the effect of this configuration on the low-speed lateral characteristics of model $B_3W_5V_5$. The results of these tests are compared with toe-in of the entire vertical tails in figure 15. These results show that toe-in produced slightly better static directional stability characteristics at the lower angles of attack (0° to 10°) associated with maximum lift-drag ratio, whereas rudder deflection produced slightly better stability at the moderate angles of attack (10° to 20°).

Vertical-tail size and shape.- The effect of various vertical tails on the lateral stability characteristics of wing-fuselage combination $B_1W_1F_2$ is shown in figure 16. In general, the directional stability increased with increase in area of the vertical tails. All the configurations except V_3 became unstable at angles of attack between 25° and 30°. This configuration differed from the others in that part of the tail extended below the wing. Comparison of the directional stability data for configurations V_2 and V_3, which are the same except for the added area below the wing for V_3, shows that the unshielded portion of fin V_3 below the wing added an almost constant increment of directional stability up to an angle of attack of 40°. The data of figure 16 also show that tail geometry had some effect on the value of C_{l_β}.

Fuselage shape.- The effect of fuselage shape on the lateral stability characteristics is shown in figure 17 for fuselages B_1, B_2, and B_3 on wing—vertical-tail combination W_5V_5. Tests were made up to an angle of attack of 30° for configurations B_1 and B_3 but only to an angle of attack of 20° for configuration B_2. In general, these differences in fuselage configuration produced only minor changes in the lateral stability characteristics.

Vertical-tail roll-out.- Outward rotation of the vertical tails has been proposed as a method of increasing the static directional stability at hypersonic speeds and at higher angles of attack. The data of figure 18 show the effect of 30° roll-out of the vertical tails on the lateral stability characteristics of configuration $B_3W_5V_6$. The static directional stability was appreciably reduced and the model became directionally unstable at a lower angle of attack than for the tails-vertical configuration. The effective dihedral was increased.

Aileron and rudder effectiveness.- The aileron and rudder effectiveness for configuration $B_3W_5V_5$ is presented in figure 19. These data show that both the aileron and rudder effectiveness remained positive over the angle-of-attack range but generally decreased with increasing angle of attack. Although the ailerons produced an appreciable amount of adverse yaw, the rudders remained effective enough to balance out the adverse yawing moment over the entire angle-of-attack range. Unpublished data from flight tests of a somewhat similar configuration have indicated that rudder and aileron characteristics of this type should provide satisfactory control over the angle-of-attack range shown.

CONCLUSIONS

The results of a low-speed investigation of the static stability and control characteristics of several configurations of a hypersonic boost-glide vehicle having a fuselage and wing-tip vertical tails on the upper surface of the wing can be summarized as follows:

1. The wing-tip vertical tails were longitudinally destabilizing.

2. Toe-in of the vertical tails increased the static directional stability.

3. Boattailing the fuselage increased the lift-drag ratio.

4. The lateral and longitudinal controls were effective over the angle-of-attack range but the effectiveness decreased at angles of attack between 20° and 30°.

5. The presence of a fuselage on the forward upper surface of the wing caused a break in the lift curve at an angle of attack of about 25° and a reduction in maximum lift coefficient.

Langley Research Center,
National Aeronautics and Space Administration,
Langley Field, Va., November 1, 1960.

REFERENCES

1. West, Franklin E., Jr., Trescot, Charles D., Jr., and Wiley, Alfred N., Jr.: Aerodynamic Characteristics for Two Hypersonic Glider Models With and Without Wing and Vertical-Tail Trailing-Edge Chord-Extensions at a Mach Number of 0.94. NASA TM X-66, 1960.

2. West, Franklin E., Jr., Trescot, Charles D., Jr., and Wiley, Alfred N., Jr.: Effect of Vertical-Tail and Rudder Deflection on the Aerodynamic Characteristics of a Hypersonic Glider Model at Mach Numbers of About 0.62 and 0.93. NASA TM X-189, 1960.

3. Ladson, Charles L., Johnston, Patrick J., and Trescot, Charles D., Jr.: Effect of Wing Plan-Form Geometry on the Aerodynamic Characteristics of a Hypersonic Glider at Mach Numbers Up to 9.6. NASA TM X-286, 1960.

4. Shanks, Robert E.: Effect of Wing Crank and Sweepback on the Low Subsonic Stability and Control Characteristics of a Model of a Hypersonic Boost-Glide Type Airplane. NASA TM X-181, 1960.

TABLE I.- GEOMETRIC CHARACTERISTICS OF TEST MODELS

Wing configuration	Area, sq in.	Span, in.	Aspect ratio	$\bar{c}$, in.	Moment reference, percent $\bar{c}$	Moment reference, percent l
W_1	704.4	26.24	0.98	34.0	48.8	64.0
W_1F_1	812.6	27.64	.94	36.9	42.0	64.0
W_1F_2	769.2	27.64	.995	34.2	43.0	64.0
W_1F_3	817.4	30.36	1.103	33.5	43.0	64.0
W_4	727.6	28.97	1.15	32.1	45.6	64.0
W_4F_2	800.6	31.18	1.26	31.7	38.6	64.0
W_5	708.6	27.49	1.07	32.1	45.8	64.0
W_6	740.2	27.48	1.02	33.02	46.3	64.0

Vertical-tail configuration	Area of each, sq in.
V_1	55.00
V_2	85.20
V_3	110.03
V_4	109.37
V_5	55.34
V_6	65.10
V_7	56.44

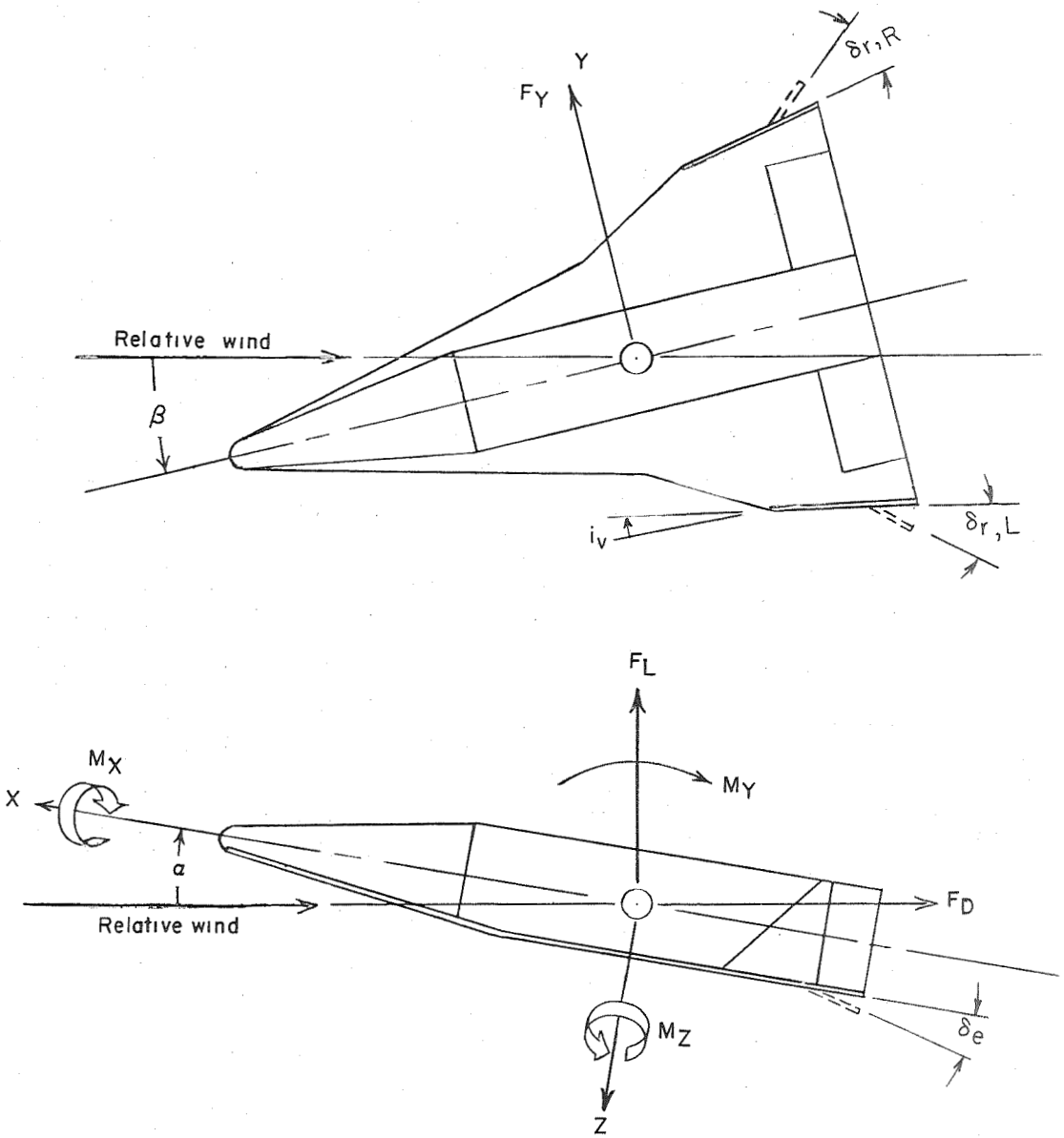

Figure 1.- Axis system used in investigation showing positive direction of forces, moments, and angles.

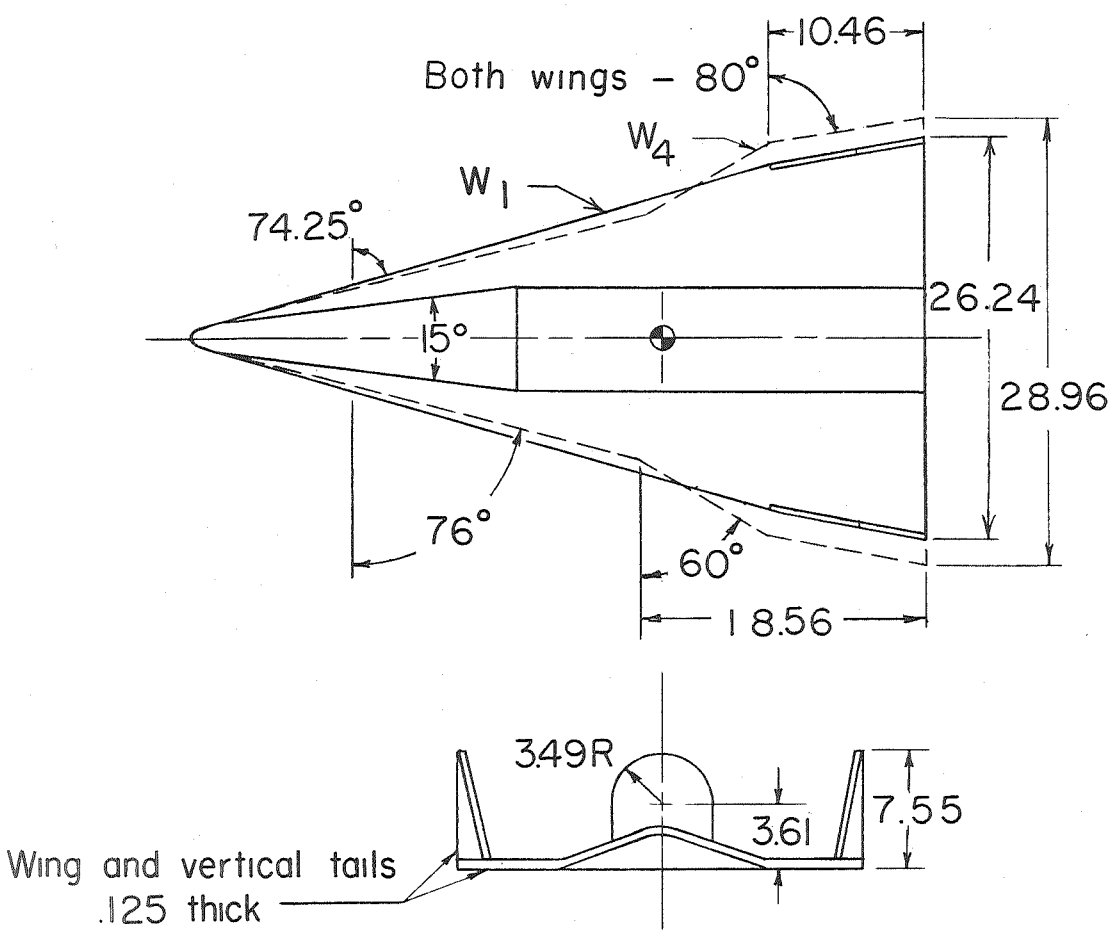

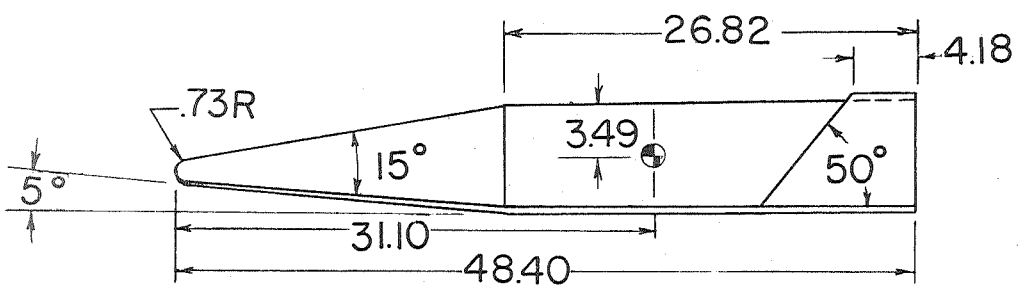

(a) Basic models.

Figure 2.- Sketch of models $B_1W_1V_1$ and $B_1W_4V_1$.

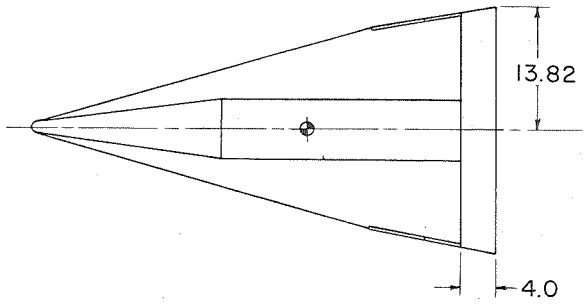

$B_1 W_1 V_1 F_1$

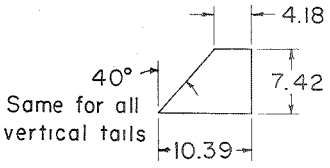

V_1

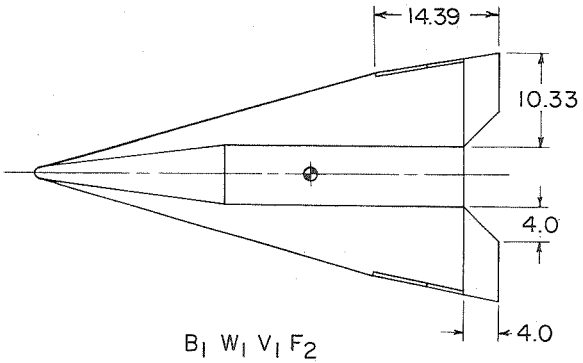

$B_1 W_1 V_1 F_2$

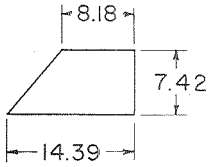

V_2

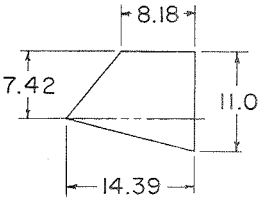

V_3

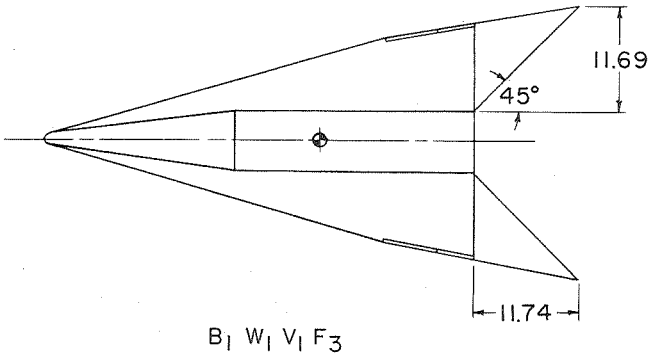

$B_1 W_1 V_1 F_3$

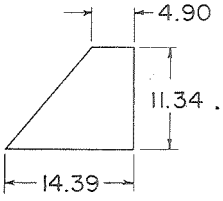

V_4

(b) Trailing-edge wing chord-extensions and vertical-tail configurations used with B_1W_1.

Figure 2.- Concluded.

L-1282

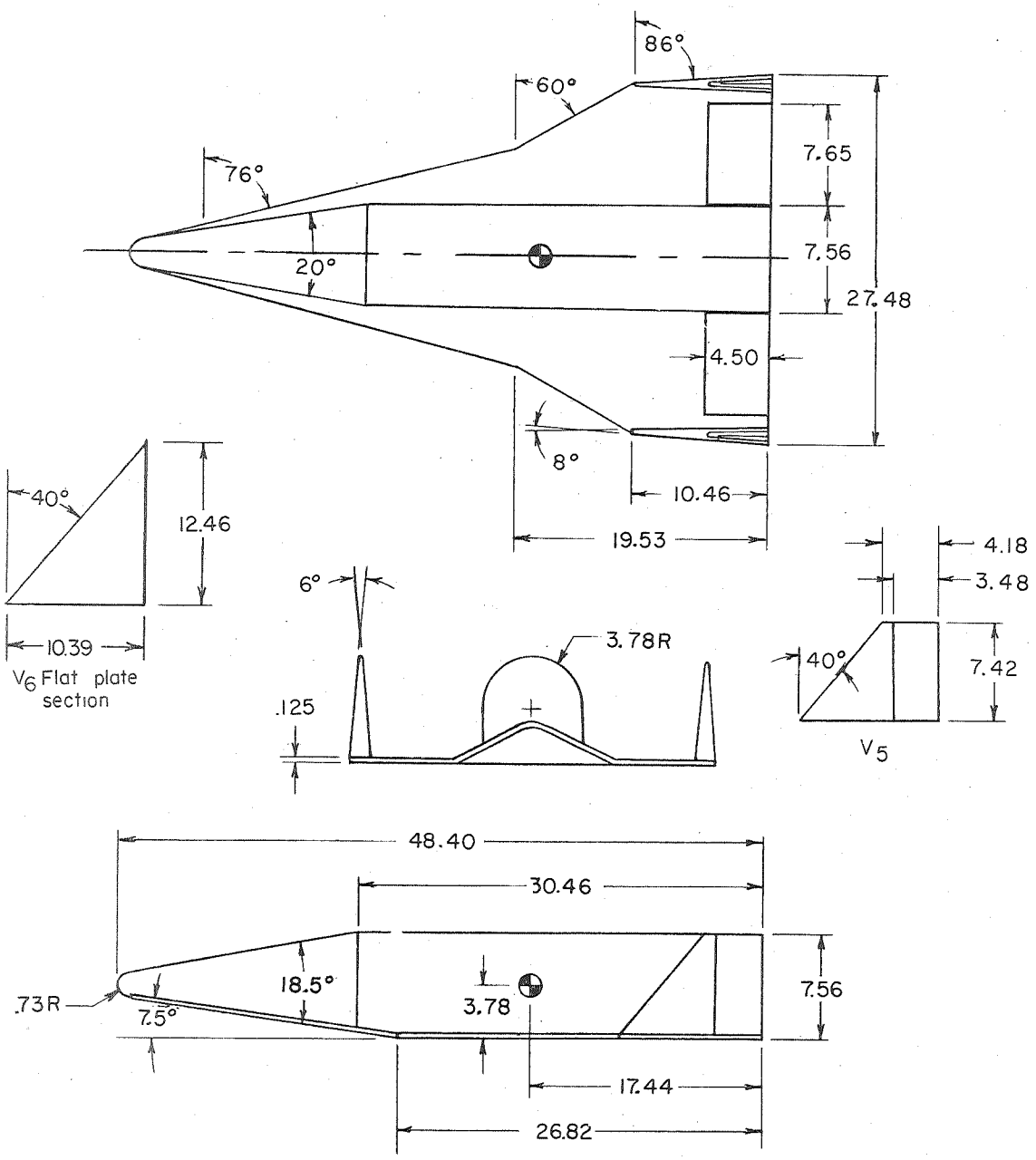

(a) Basic fuselage B_2.

Figure 3.- Sketch of model $B_2W_5V_5$.

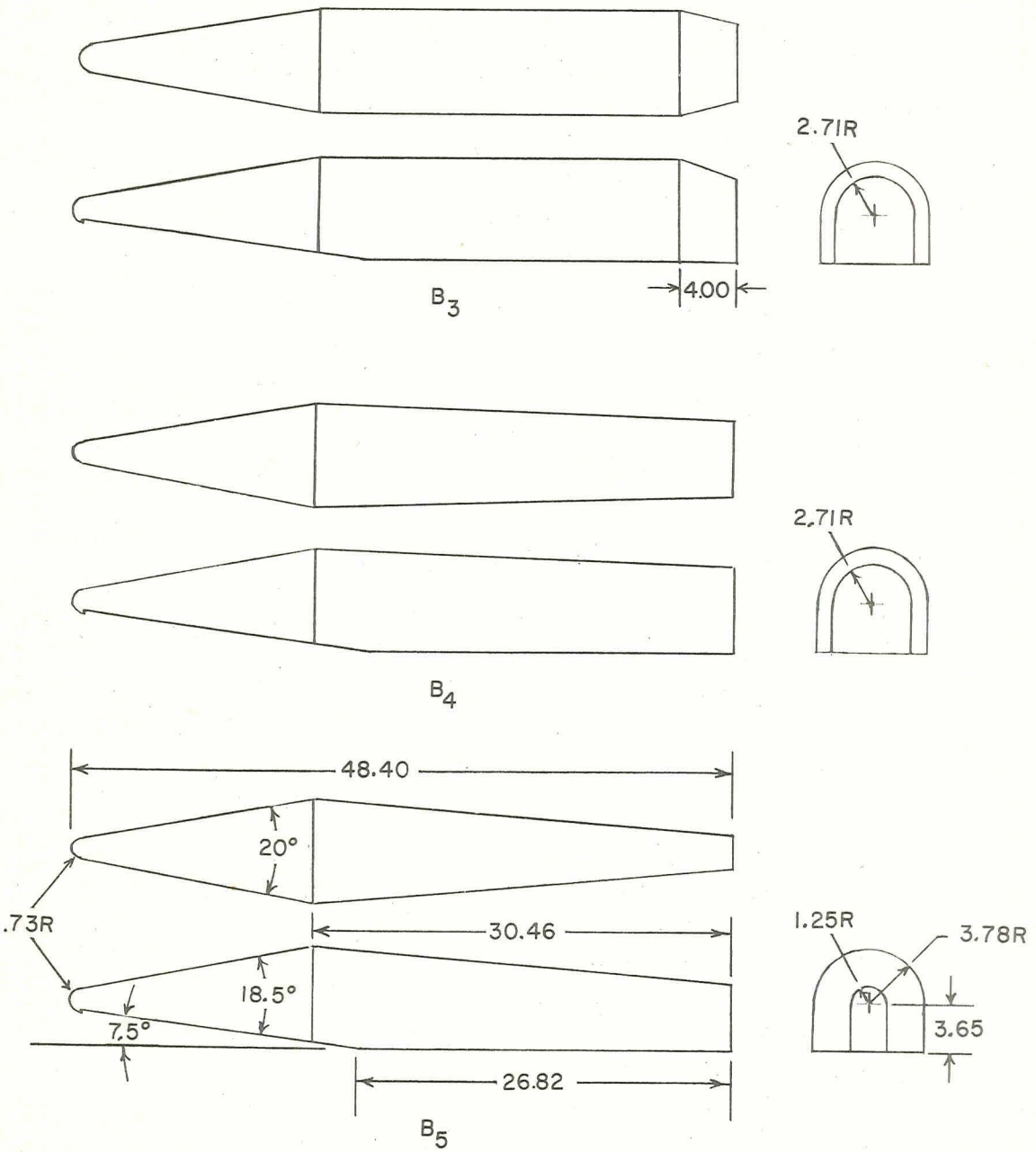

(b) Fuselages B_3, B_4, and B_5. Dimensions shown in side and top views of B_5 are same for fuselages B_3 and B_4.

Figure 3.- Concluded.

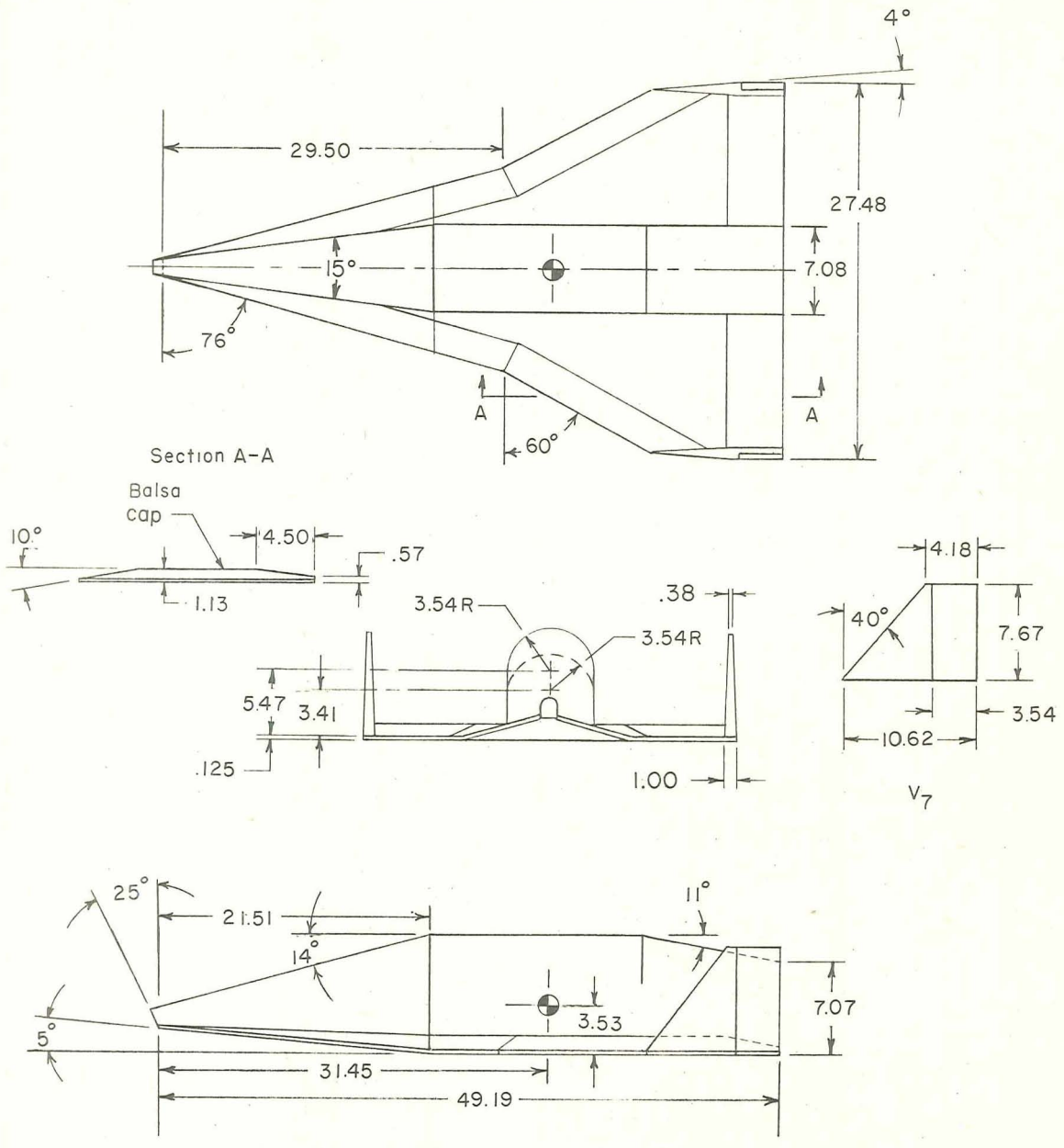

Figure 4.- Sketch of model $B_6W_6V_7$.

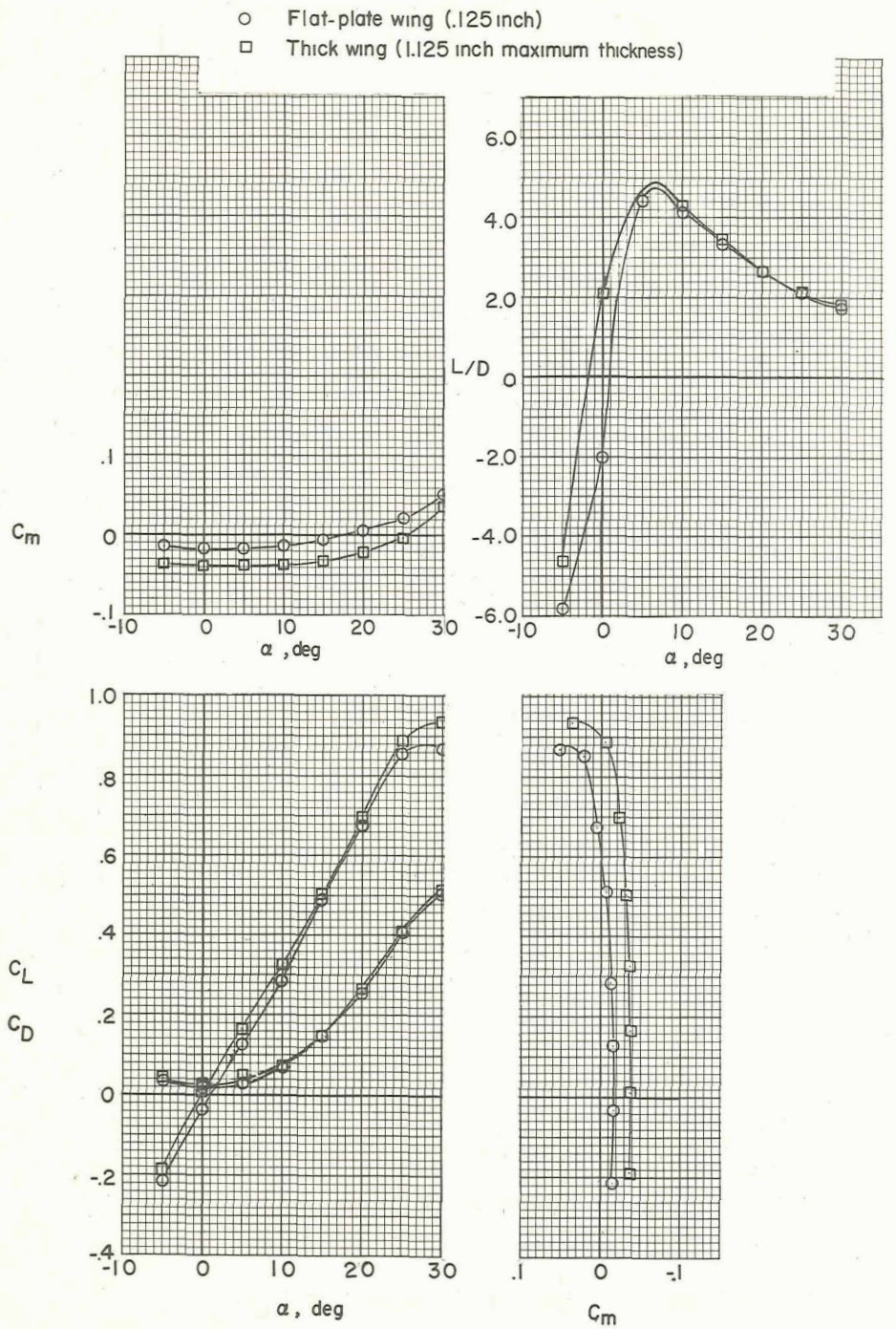

Figure 5.- Comparison of the static longitudinal characteristics of model $B_6W_6V_7$ with flat-plate wing and thick cambered wing. 0° toe; $\beta = 0°$.

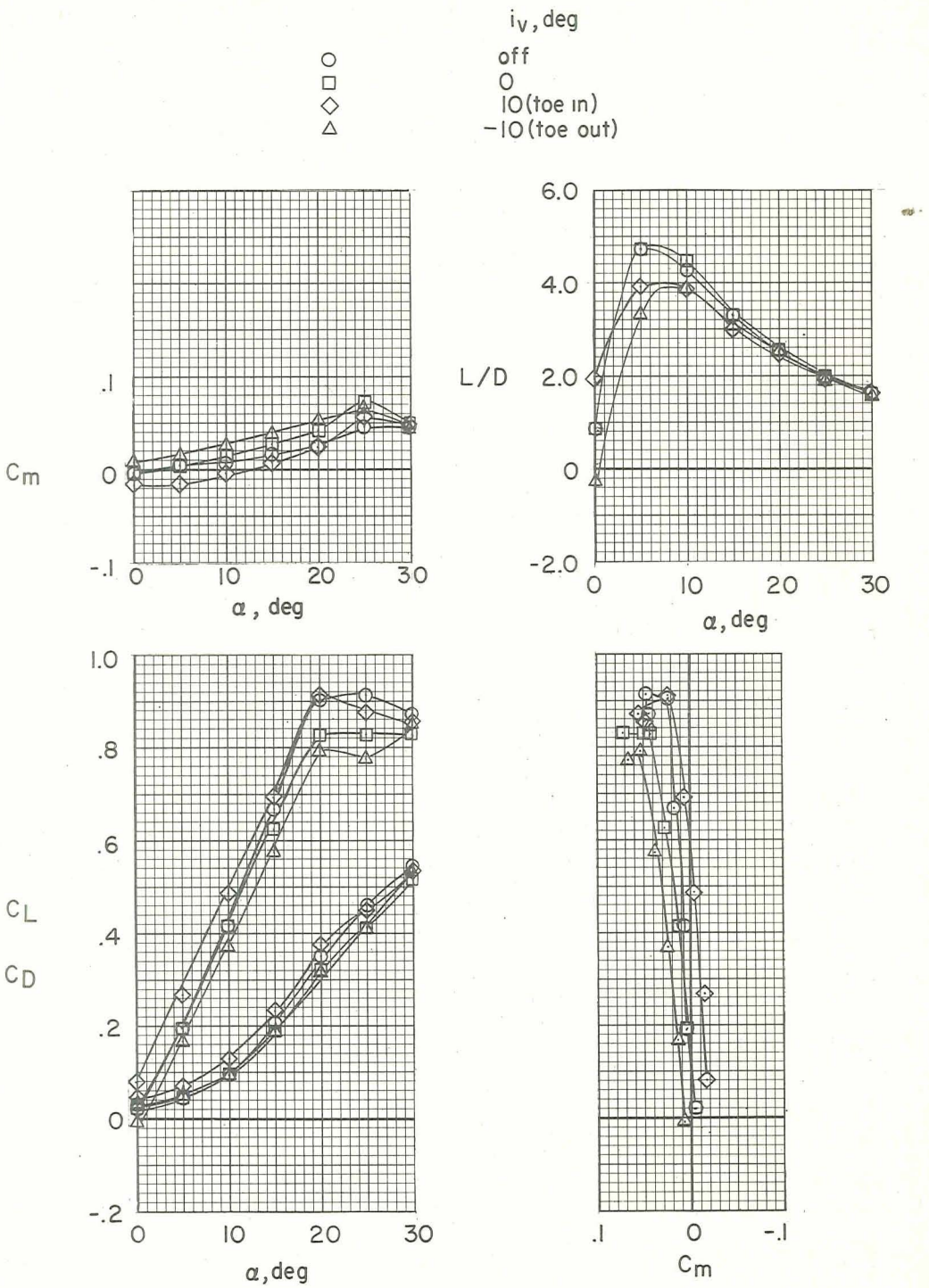

Figure 6.- Effect of vertical-tail toe angle on longitudinal characteristics of model $B_1W_4V_1$. $\beta = 0^\circ$.

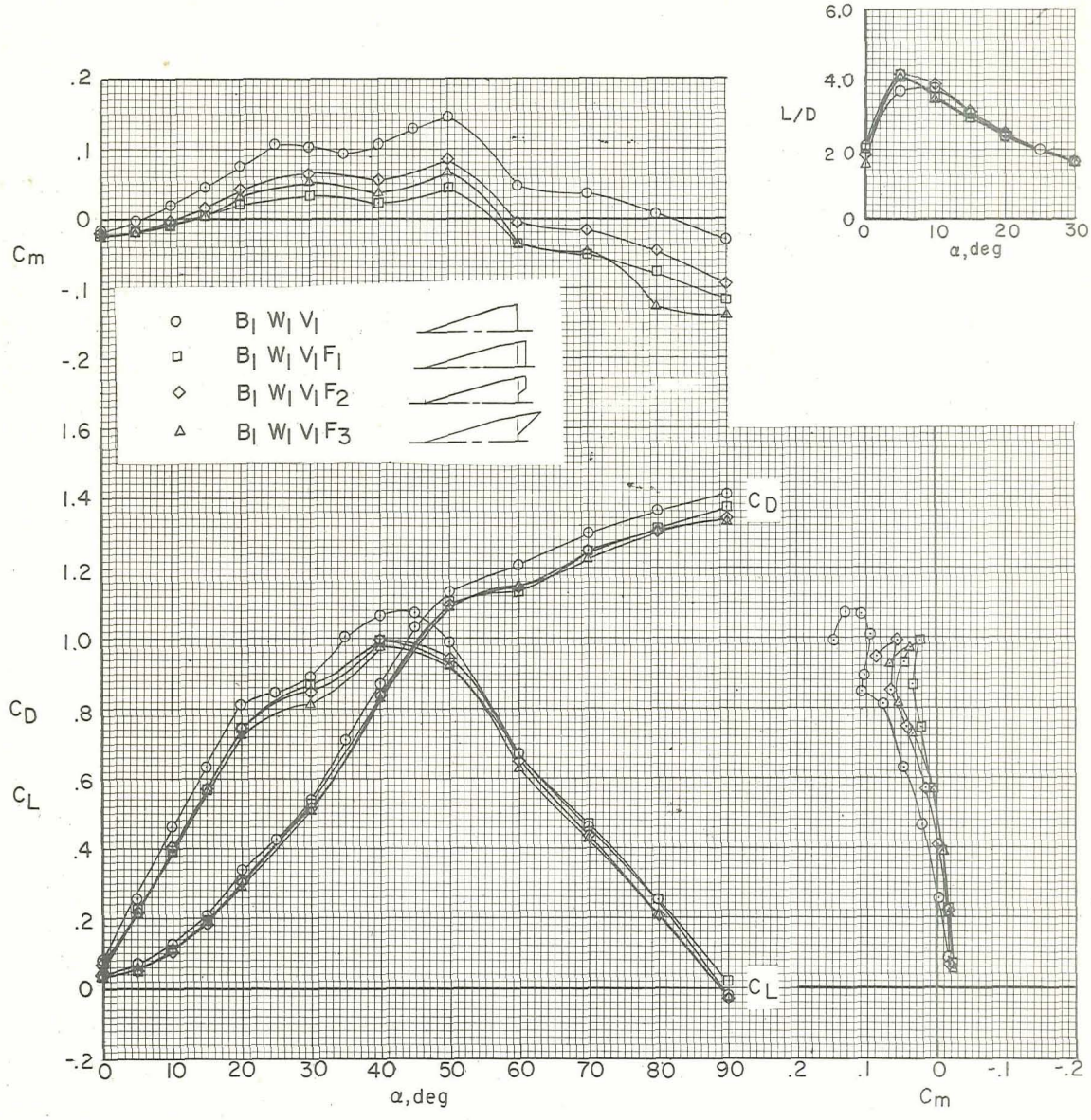

(a) Pitching moments referred to 0.64l.

Figure 7.- Longitudinal characteristics of model $B_1W_1V_1$ with three trailing-edge chord-extension configurations. 10° toe in; $\beta = 0°$.

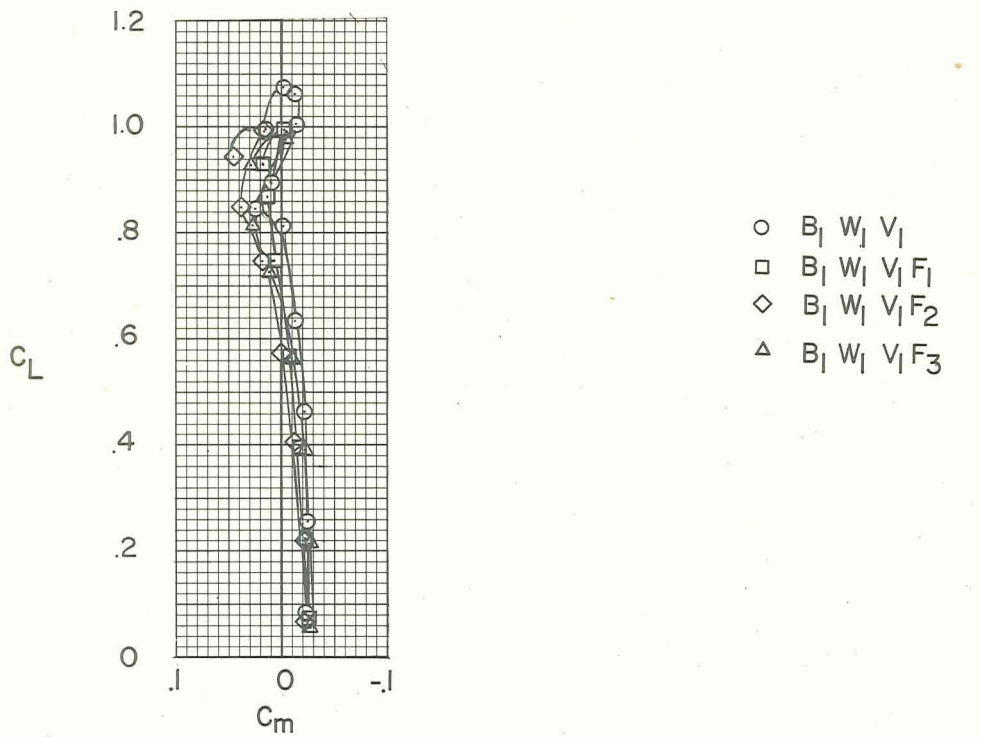

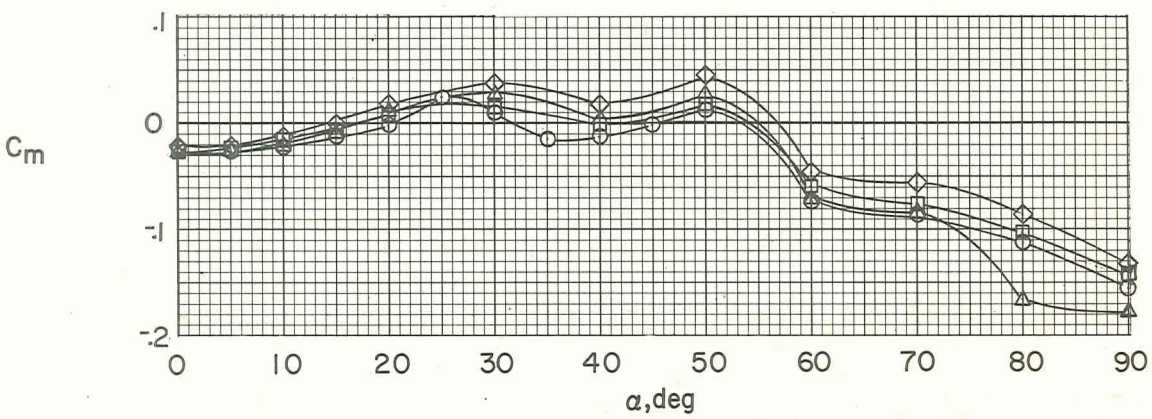

(b) Pitching moments referred to $0.40\bar{c}$.

Figure 7.- Concluded.

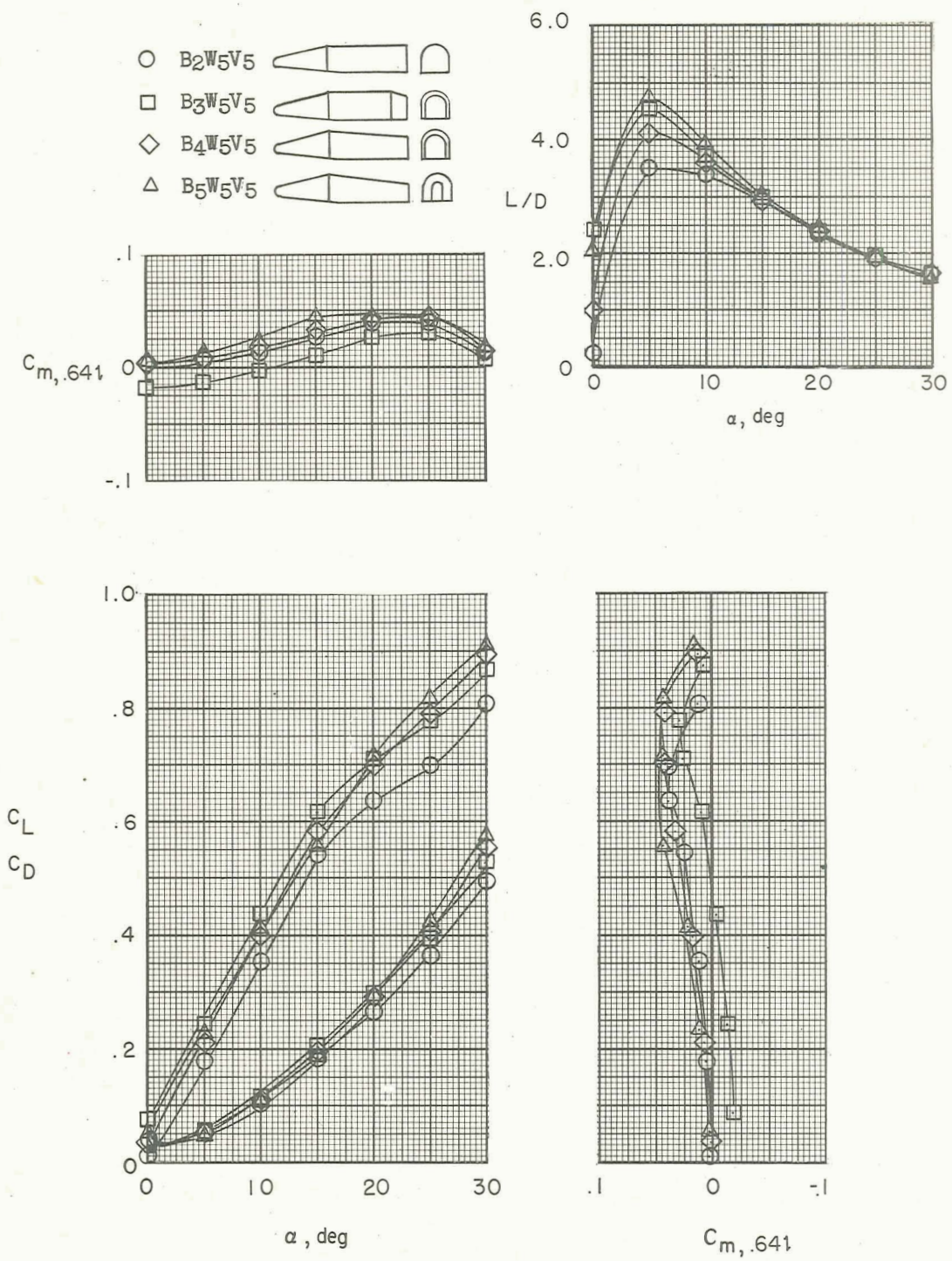

Figure 8.- Effect of fuselage shape on longitudinal characteristics of wing-tail combination W_5V_5. 0^o toe; $\beta = 0^o$.

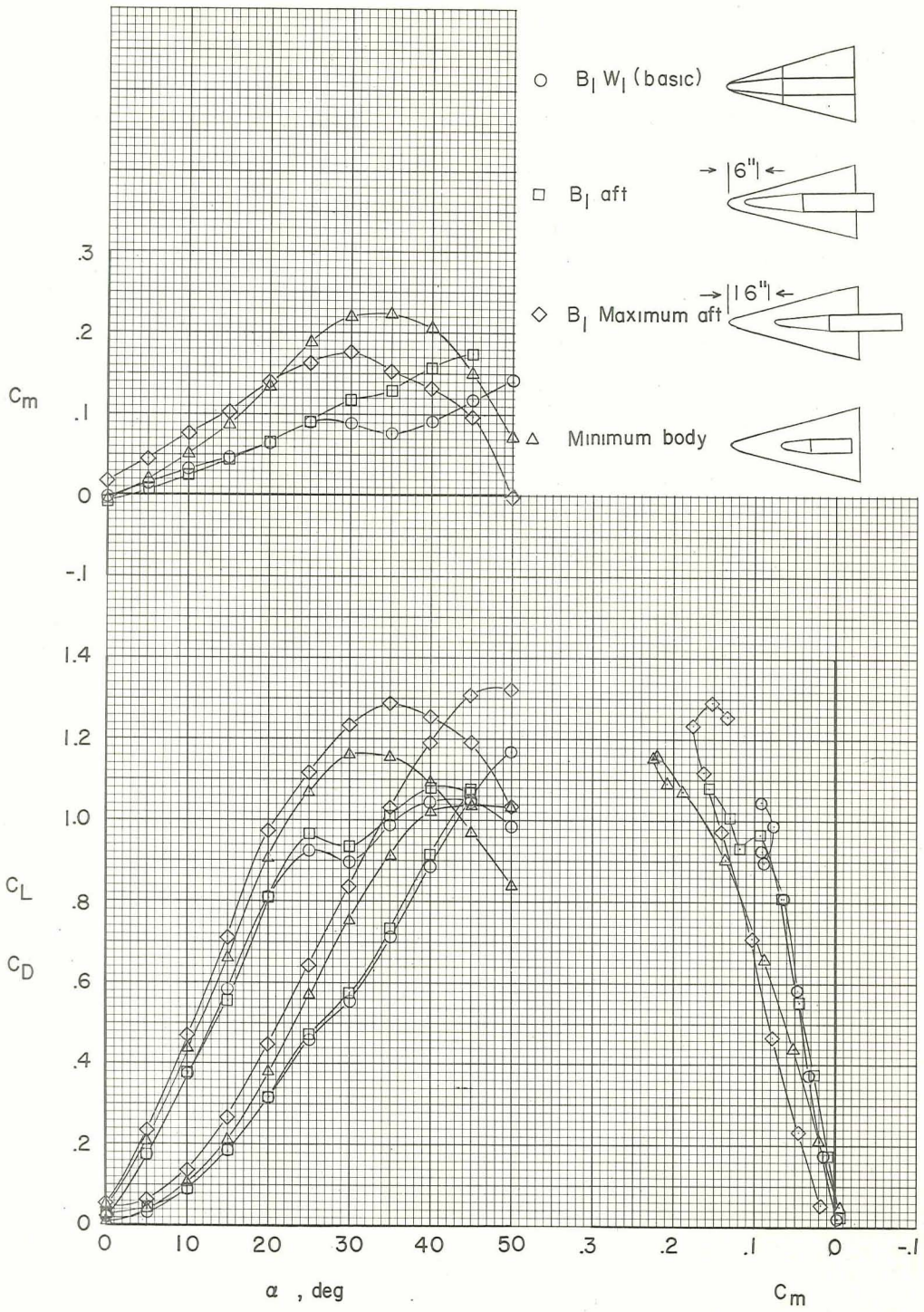

Figure 9.- Effect of fuselage location on the longitudinal characteristics of model $B_1W_1V_1$. 10° toe in.

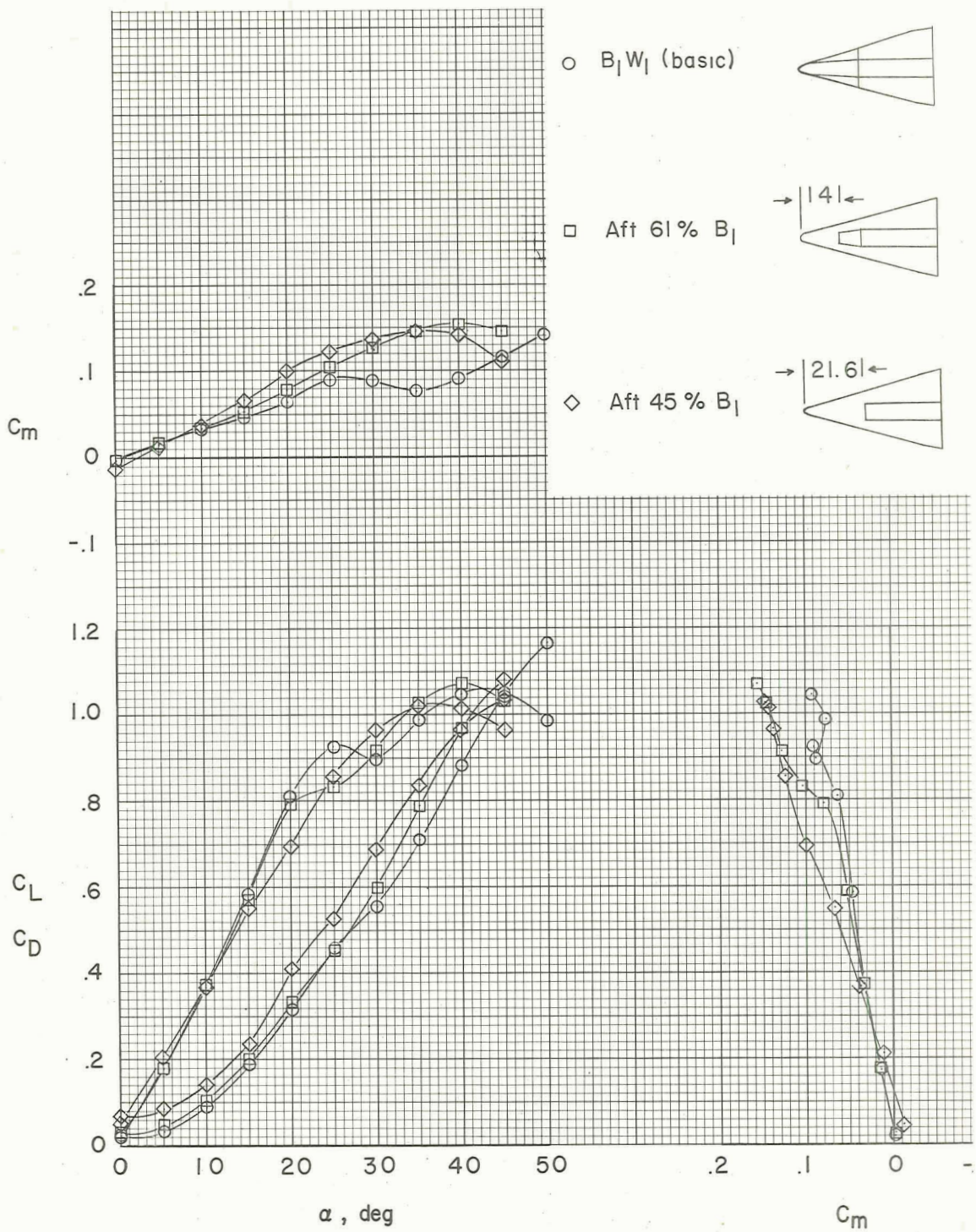

L-1282

Figure 10.- Effect of size of conical forward fuselage on the longitudinal characteristics of model $B_1W_1V_1$. 10° toe in.

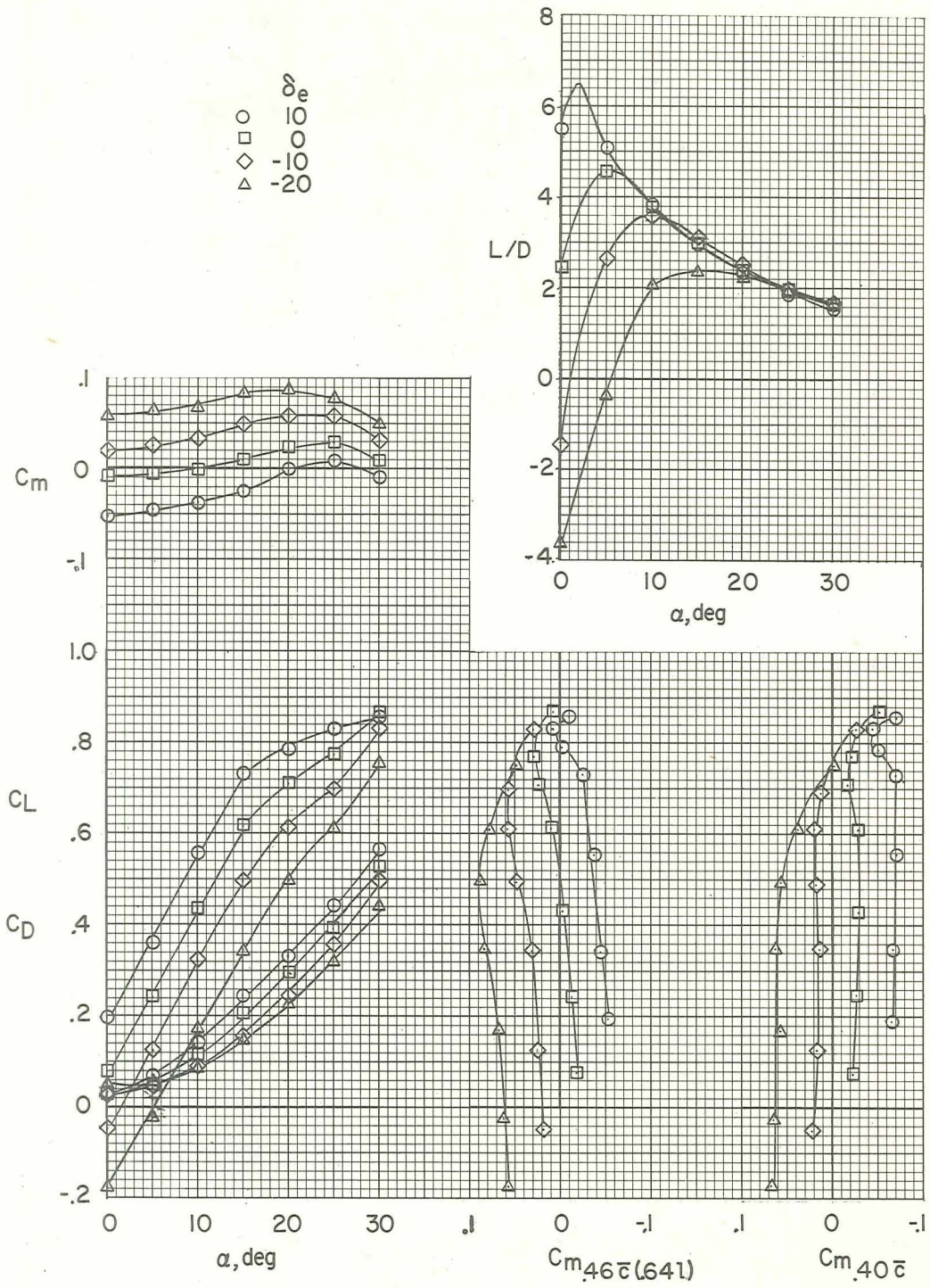

Figure 11.- Longitudinal characteristics of configuration $B_3W_5V_5$. 0° toe; $\beta = 0^\circ$.

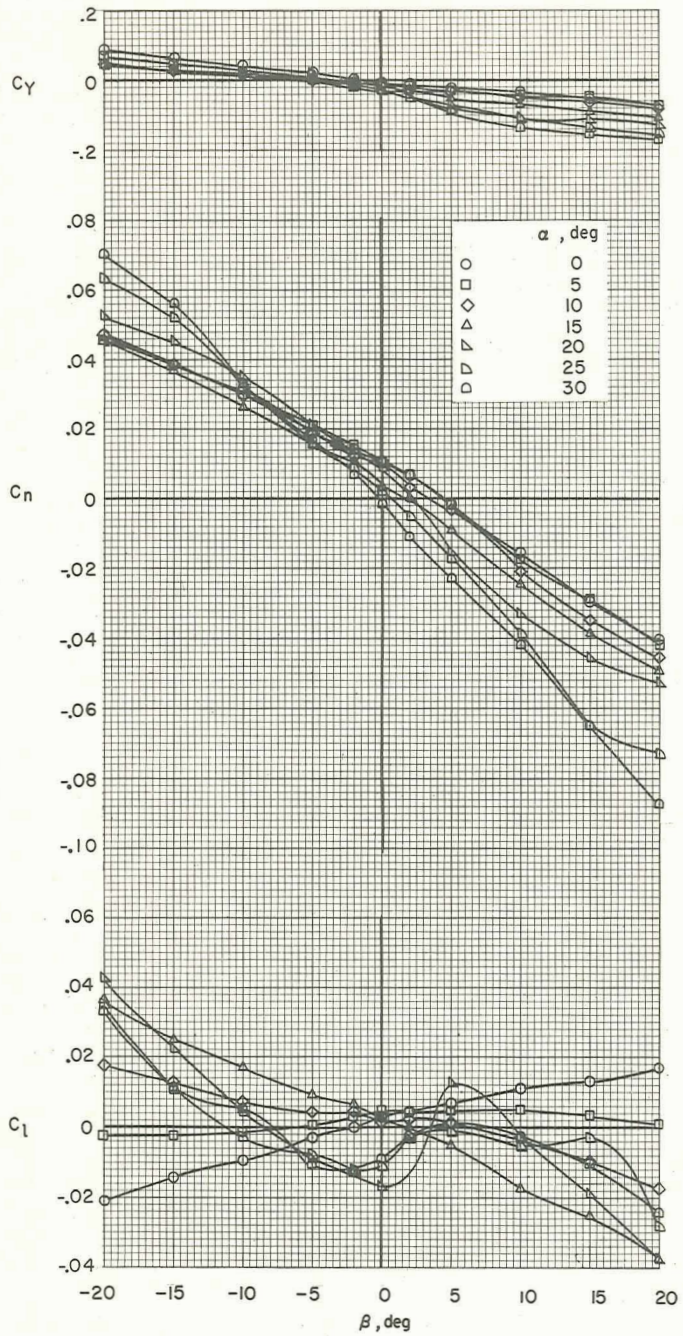

(a) B_3W_5.

Figure 12.- Variation of the static lateral coefficients with angle of sideslip. $\delta_e = 0^\circ$.

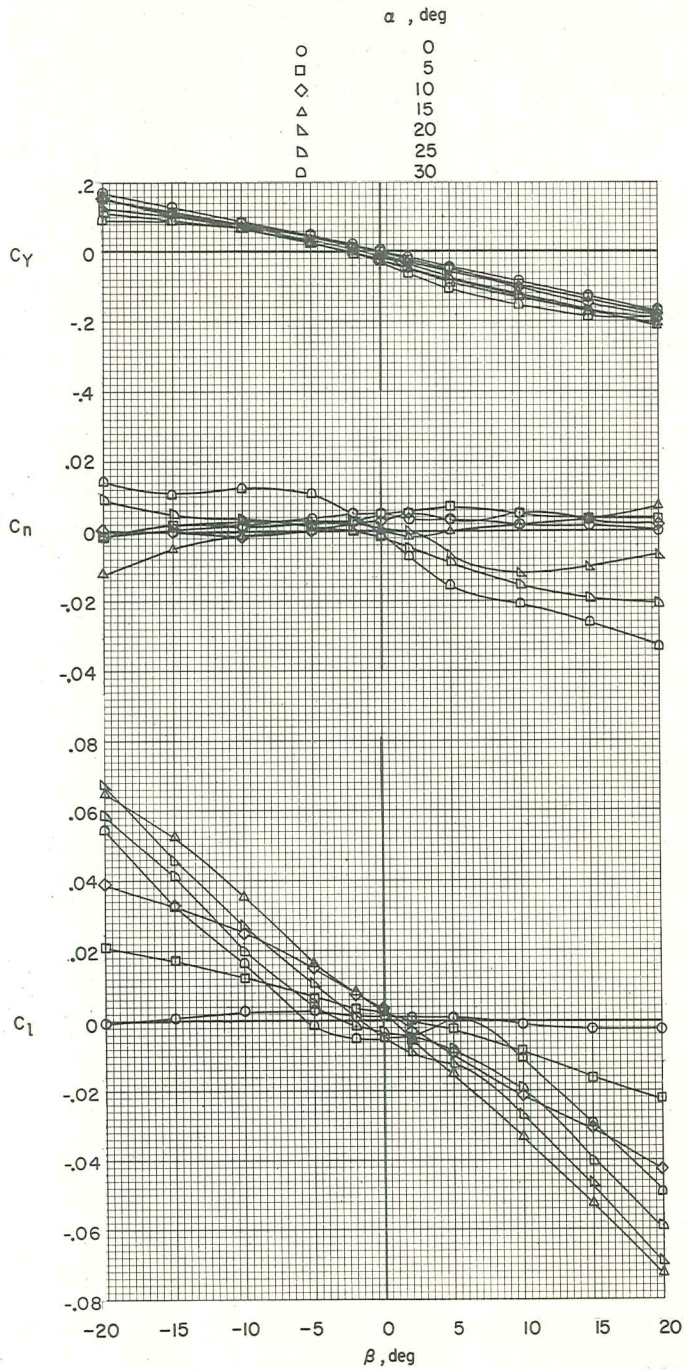

(b) $B_3W_5V_1$; 0° toe angle.

Figure 12.- Continued.

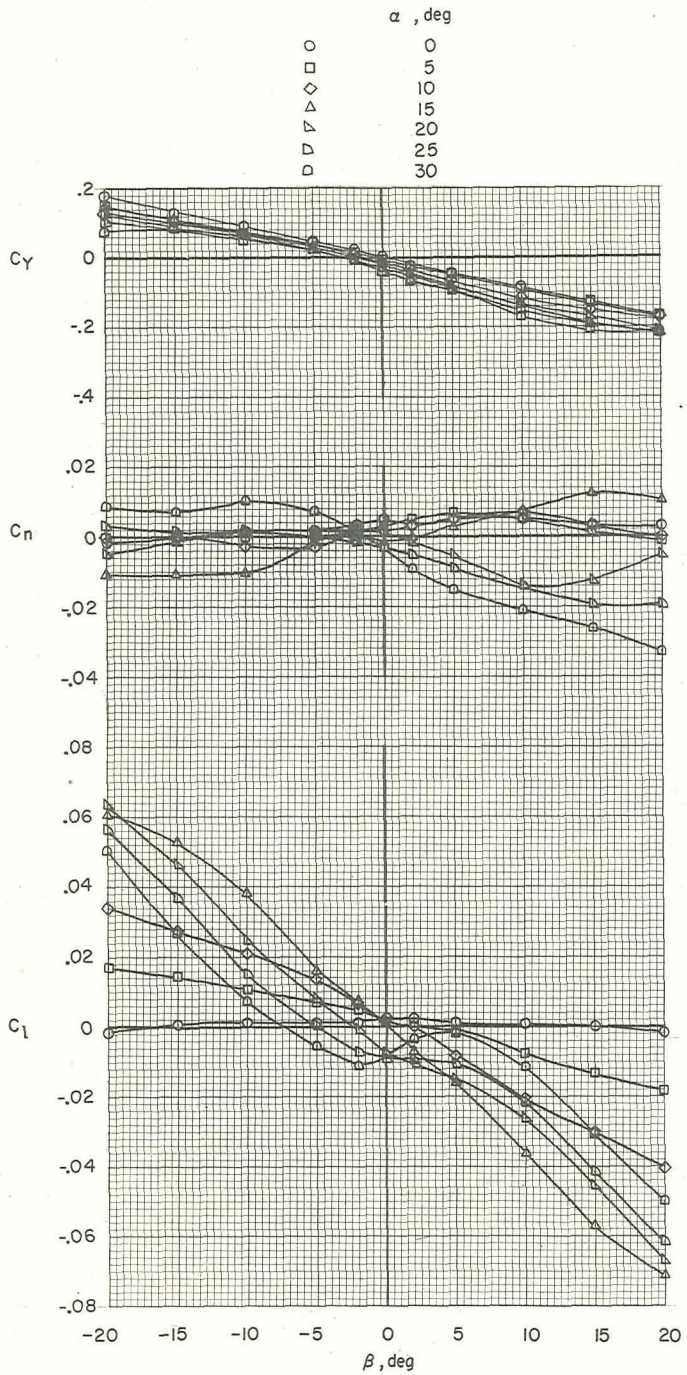

(c) $B_3W_5V_1$; 4° toe-in.

Figure 12.- Continued.

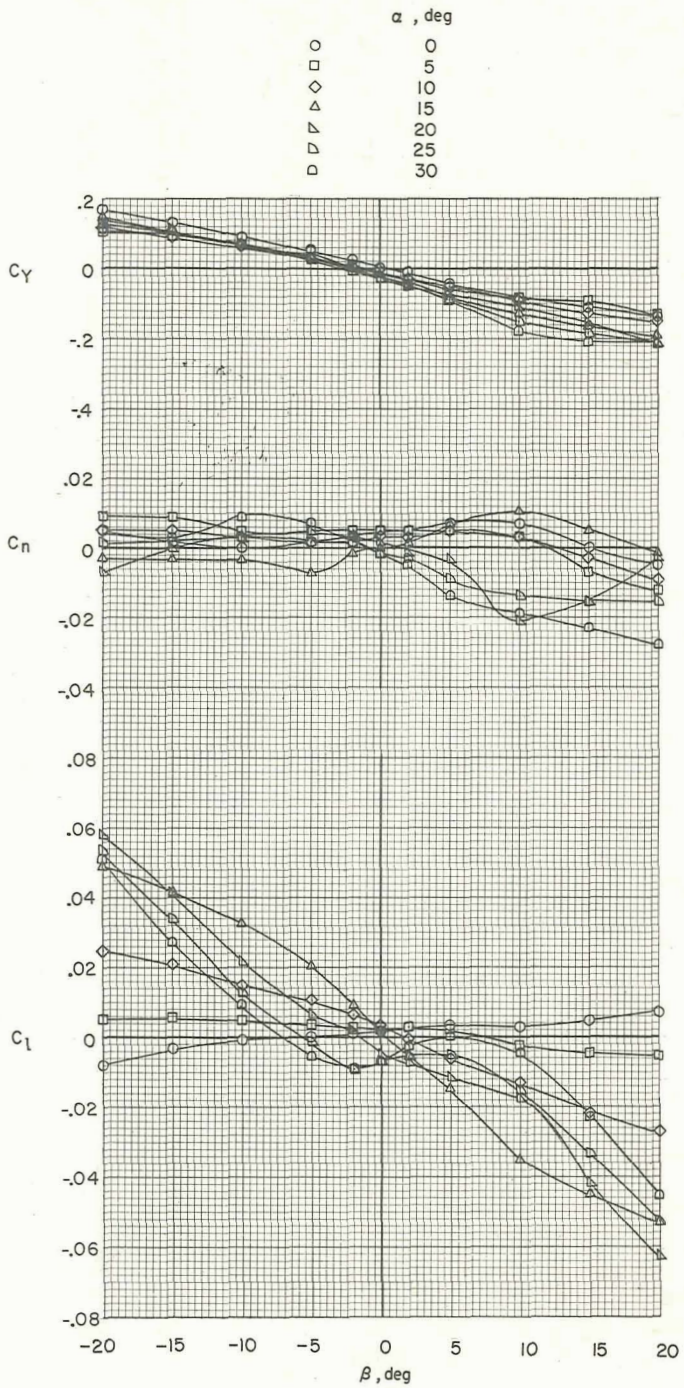

(d) $B_3W_5V_1$; 10° toe-in.

Figure 12.- Continued.

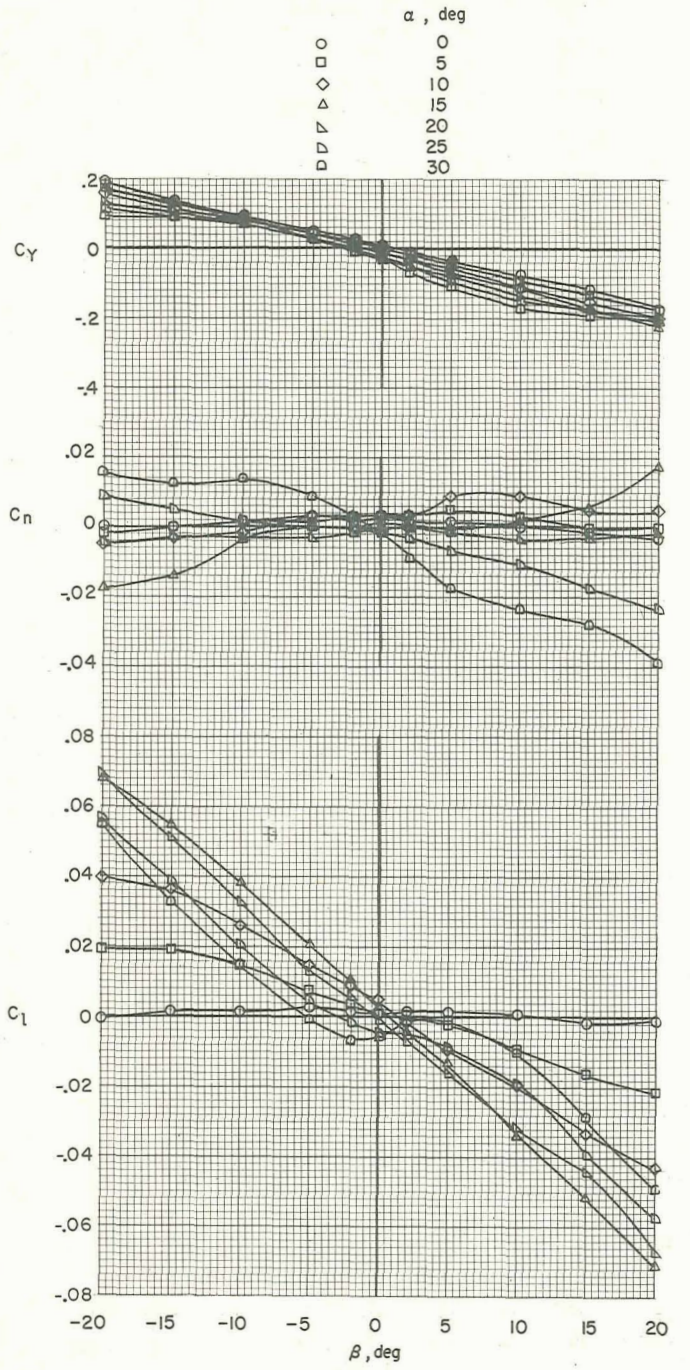

(e) $B_3W_5V_5$.

Figure 12.- Continued.

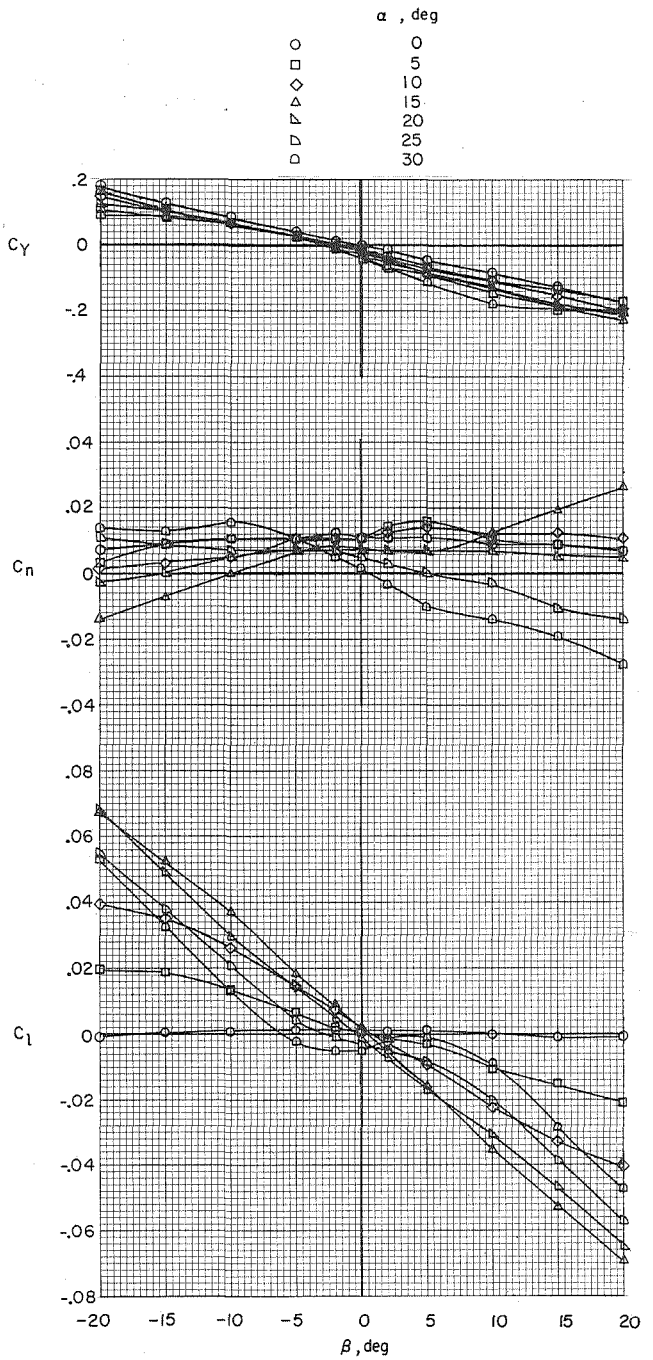

(f) $\beta_3 W_5 V_5$; $\delta_{r,R} = \delta_{r,L} = 10^\circ$.

Figure 12.- Continued.

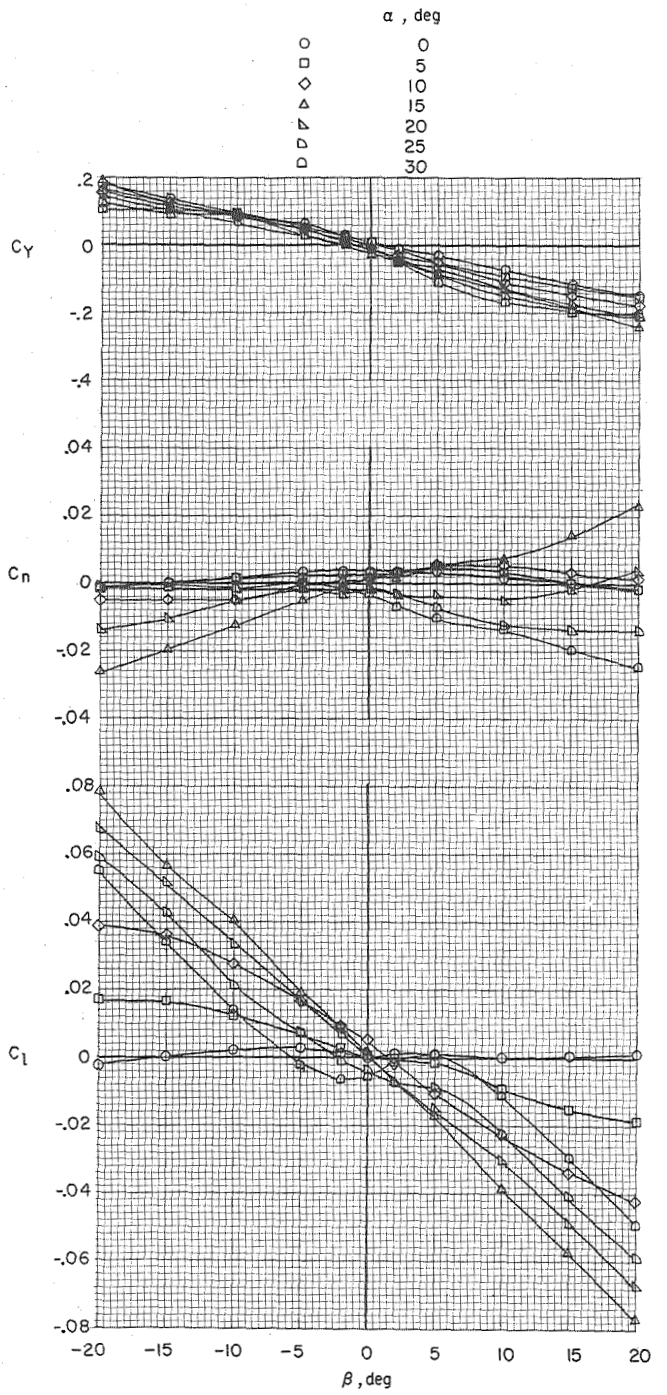

(g) $B_3W_5V_5$; $\delta_{r,R} = \delta_{r,L} = 20^\circ$.

Figure 12.- Continued.

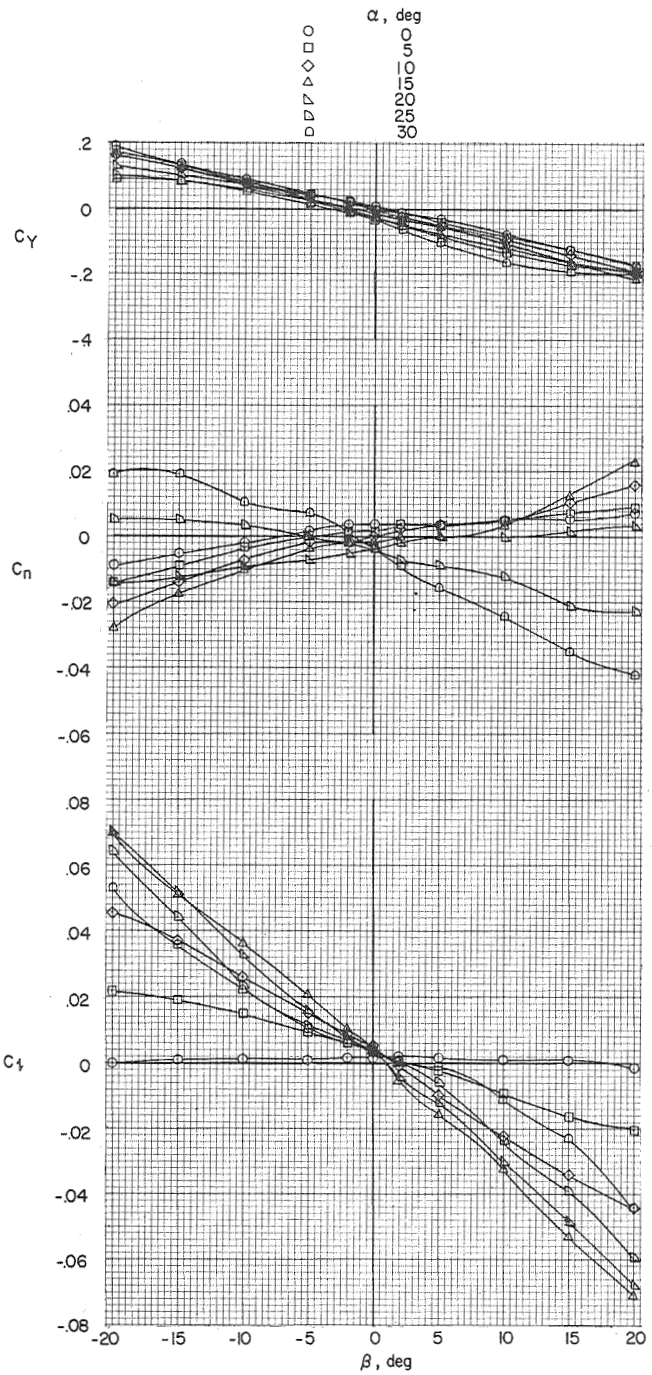

(h) $B_1W_5V_5$.

Figure 12.- Continued.

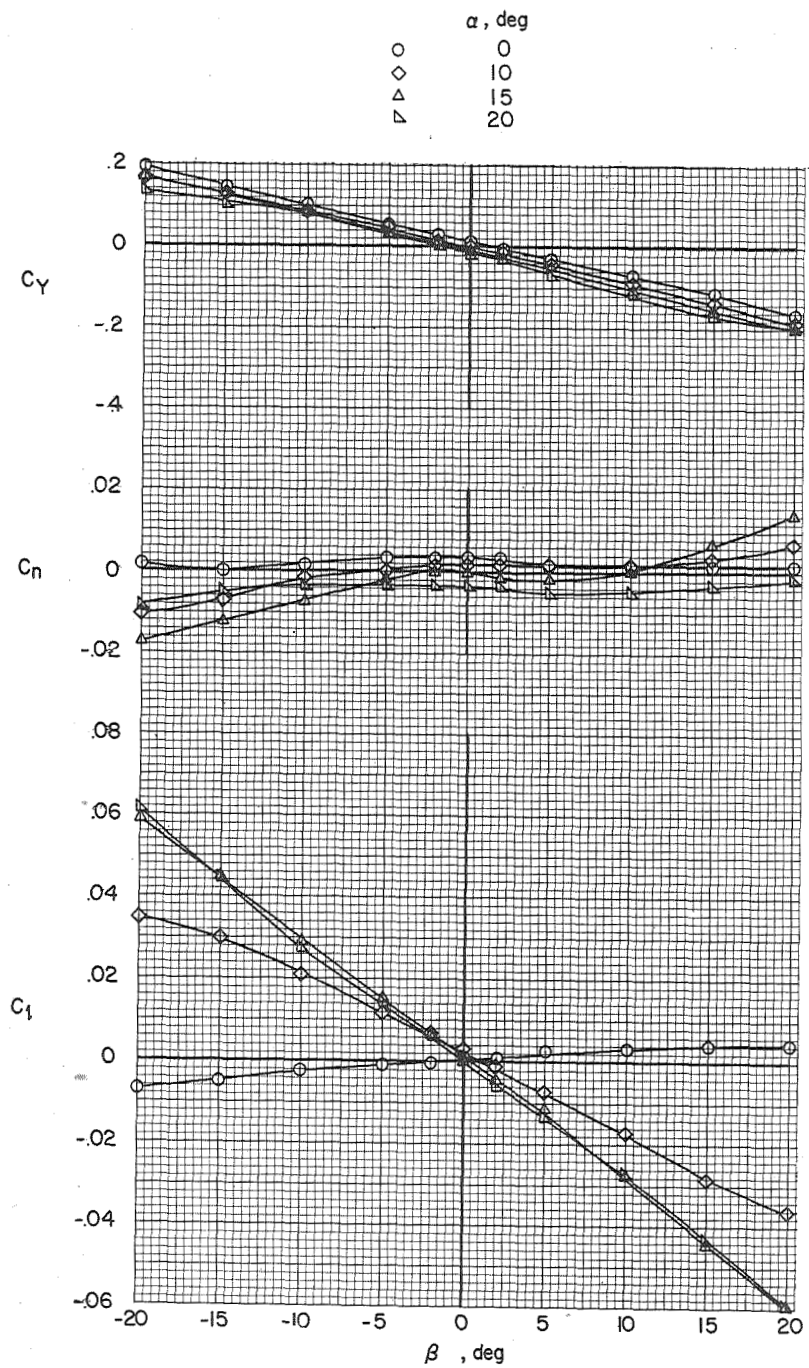

(i) $B_2W_5V_5$.

Figure 12.- Continued.

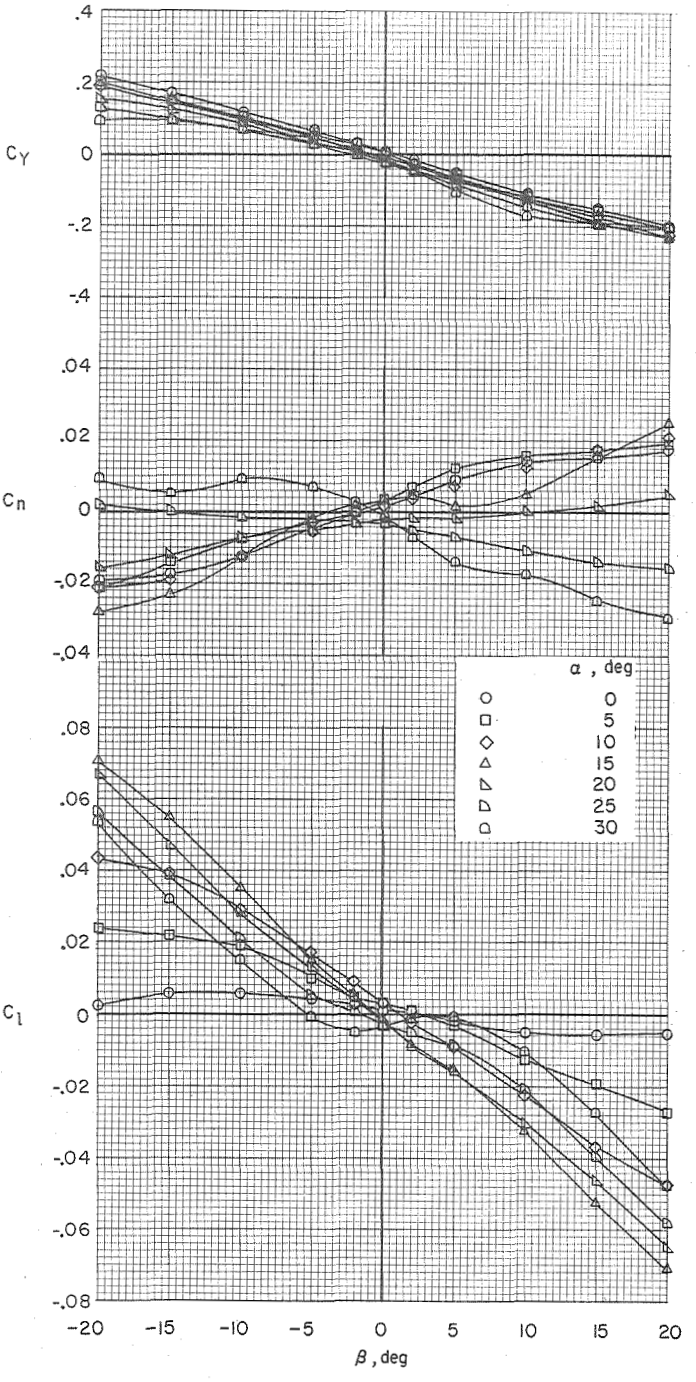

(j) $B_3W_5V_6$.

Figure 12.- Continued.

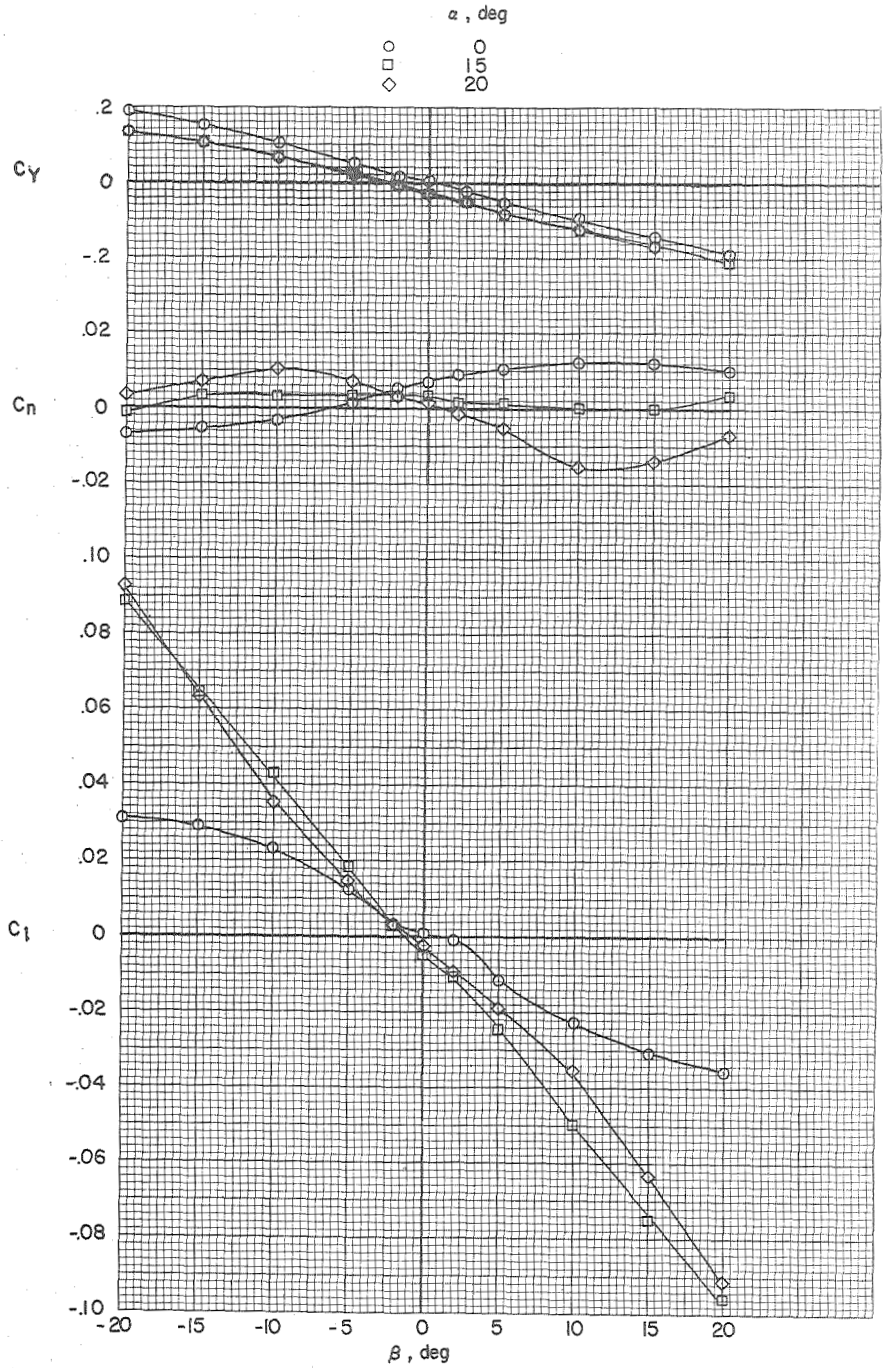

(k) $B_3W_5V_6$; V_6 rolled out 30°.

Figure 12.- Concluded.

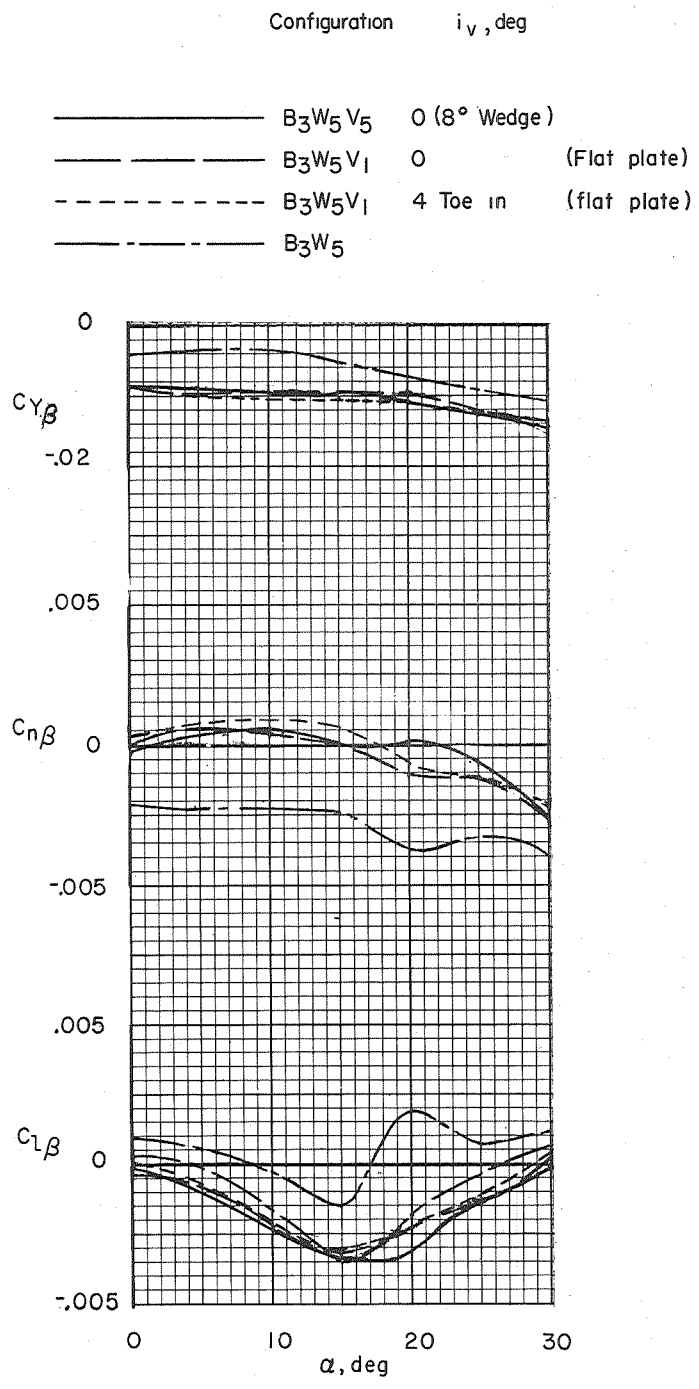

Figure 13.- Comparison of the lateral characteristics of vertical tails V_1 (flat plate) at two toe angles with vertical tails V_5 (8° wedge section).

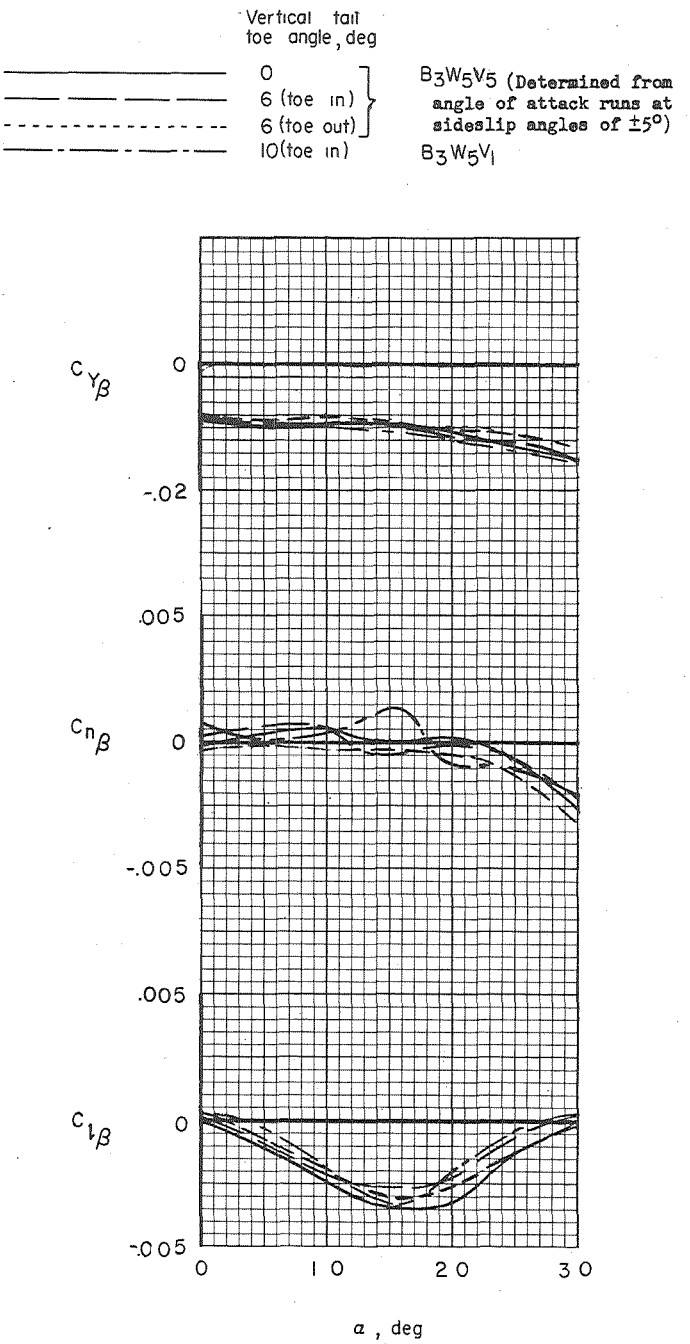

(a) Models $B_3W_5V_5$ and $B_3W_5V_1$.

Figure 14.- Effect of vertical-tail toe angle on the lateral stability characteristics.

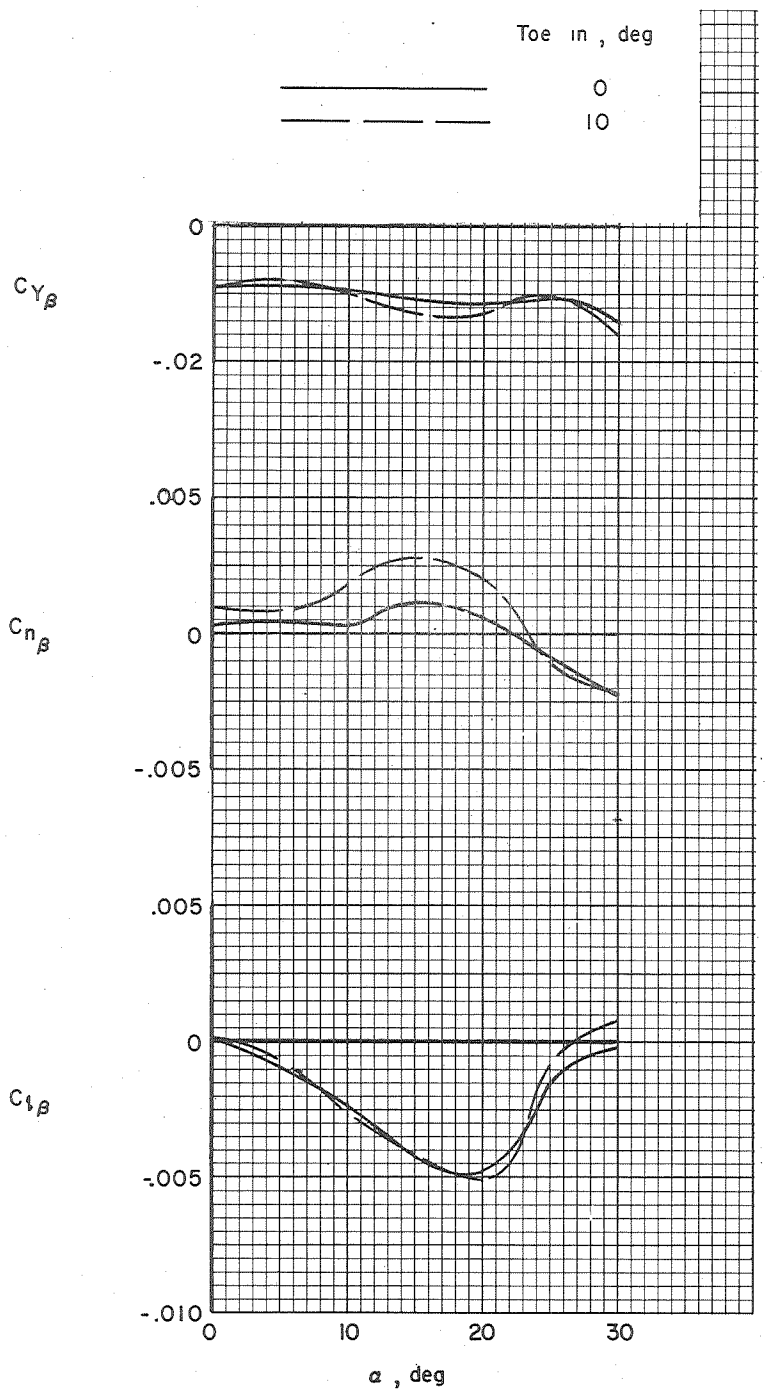

(b) Model $B_1W_4V_1$.

Figure 14.- Concluded.

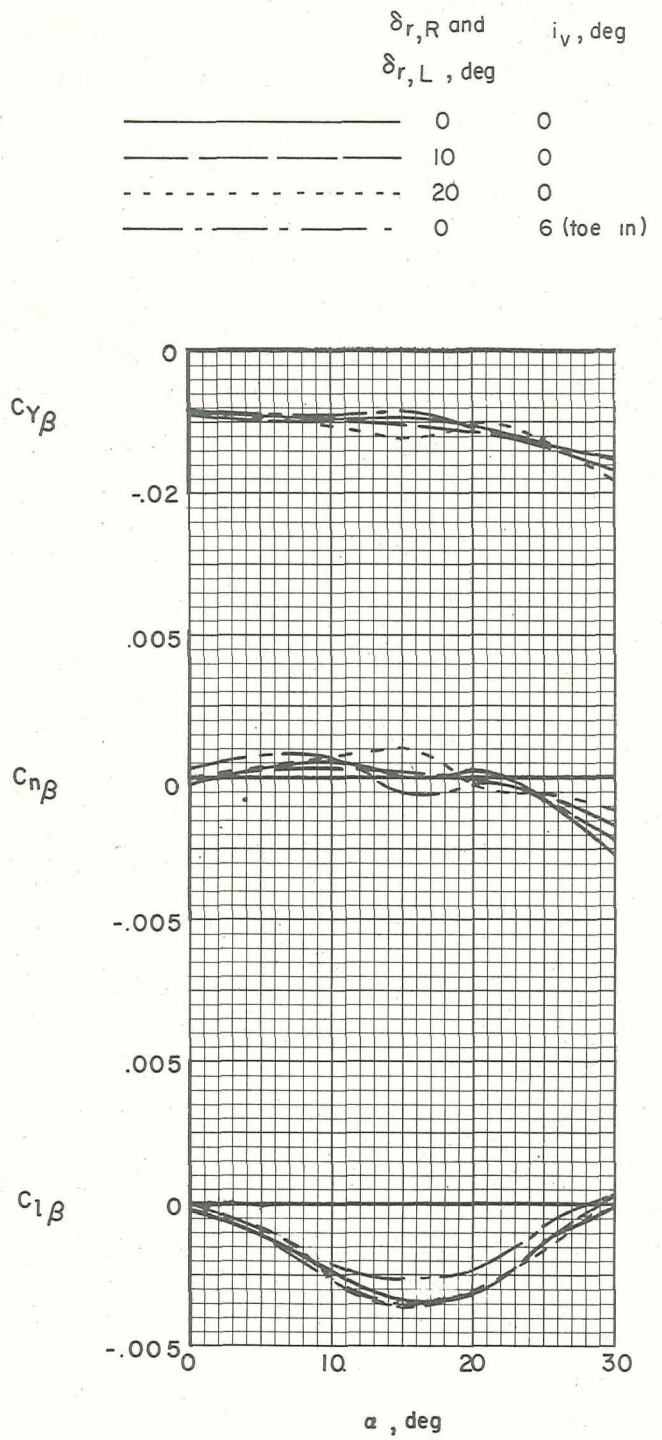

Figure 15.- Effect of vertical-tail toe-in and outward deflection of both rudders on lateral stability characteristics. Model $B_3W_5V_5$.

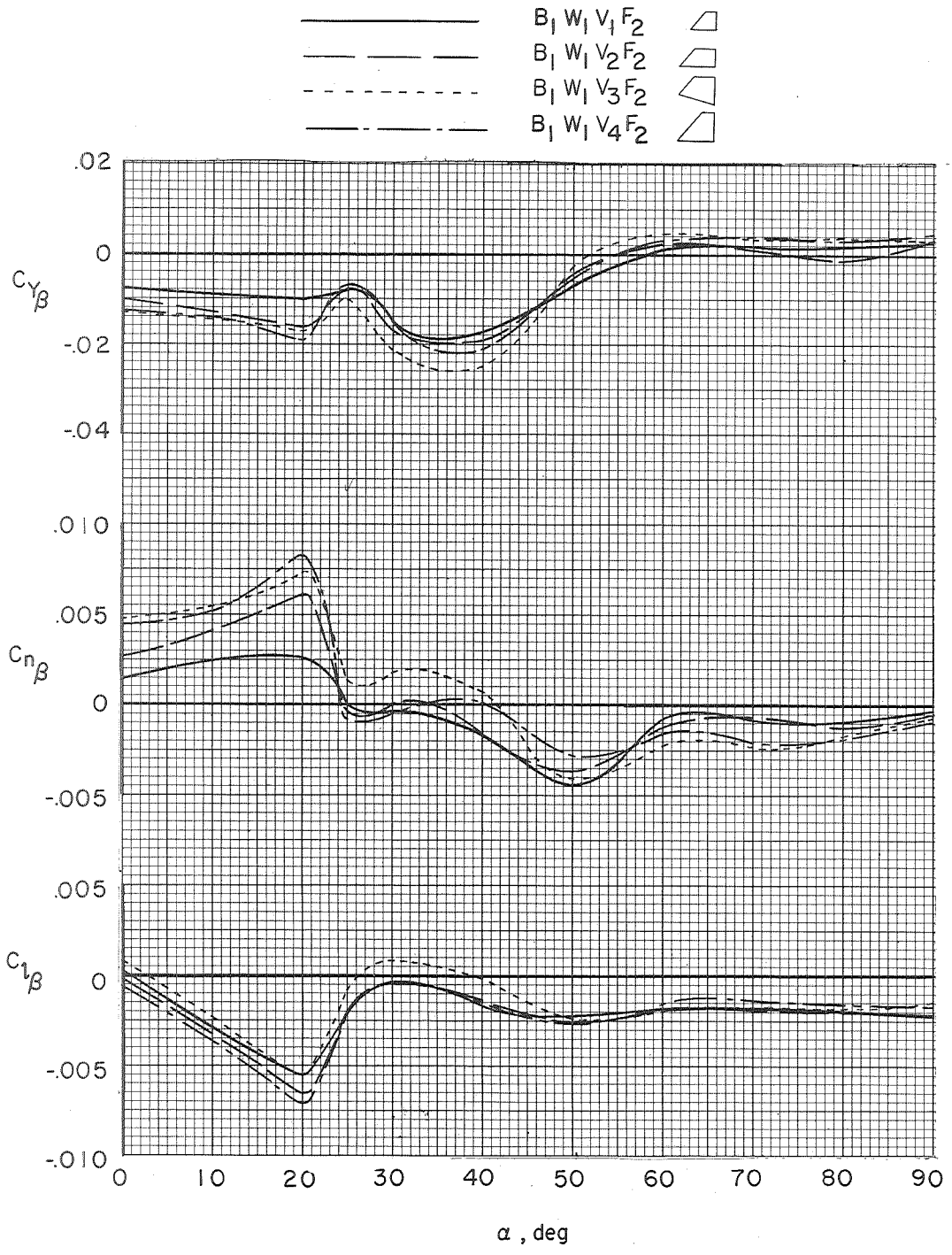

Figure 16.- Variation of static lateral stability derivatives with angle of attack for various vertical-tail configurations. 10° toe-in.

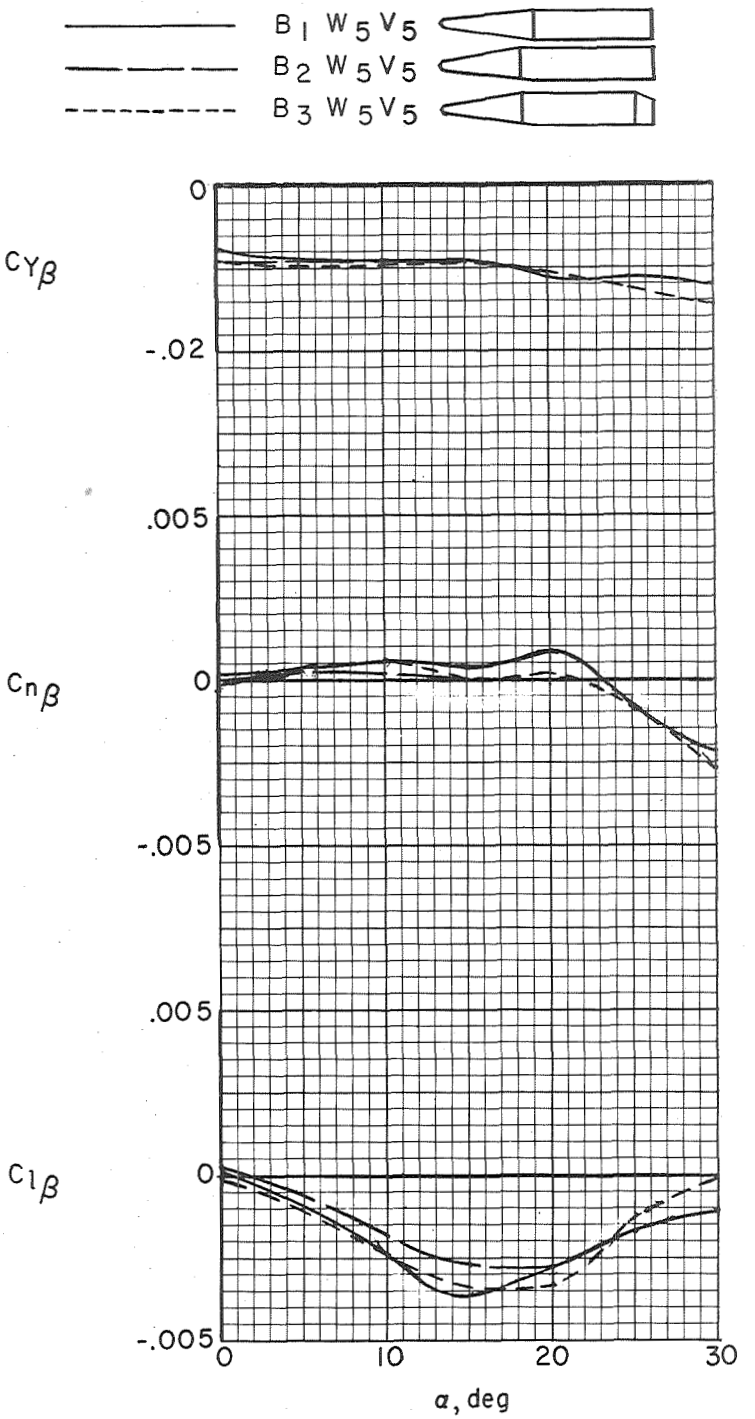

Figure 17.- Effect of fuselage shape on the lateral stability characteristics of wing-tail combination W_5V_5. 0° toe-in.

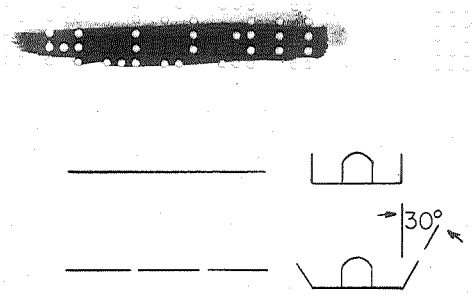

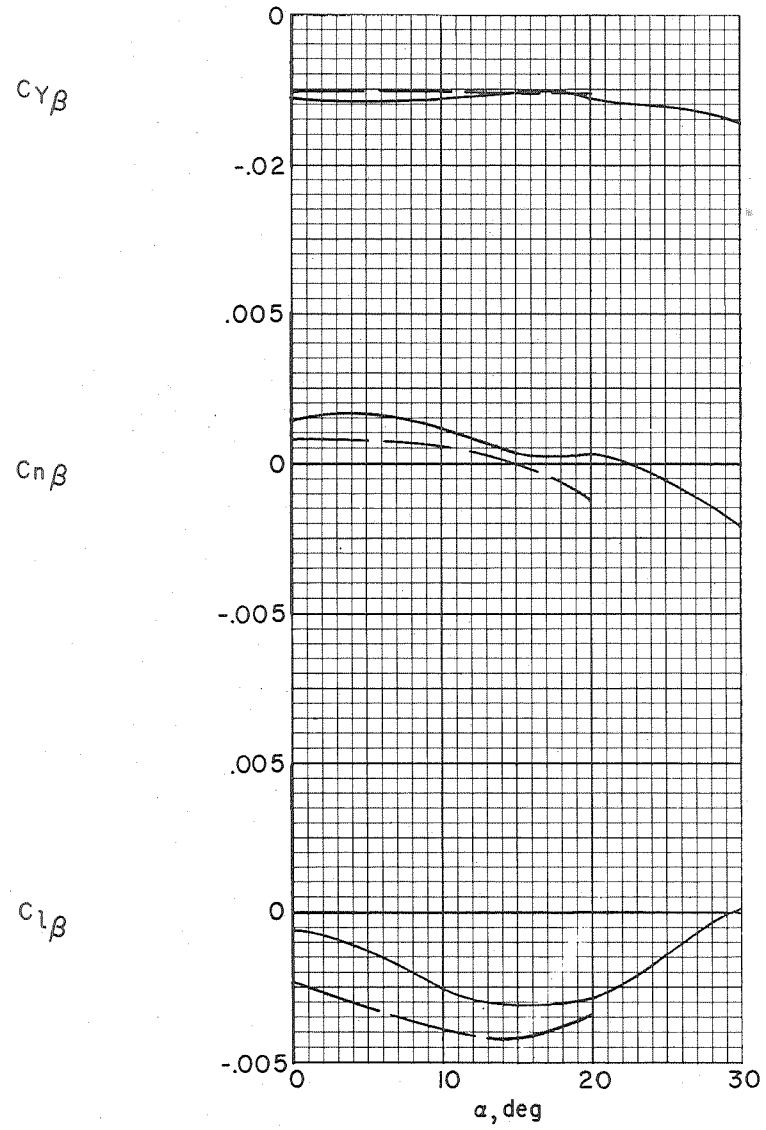

Figure 18.- Effect of 30° outward rotation of vertical tail on the lateral stability characteristics of configuration $B_3W_5V_6$. 4° toe-in.

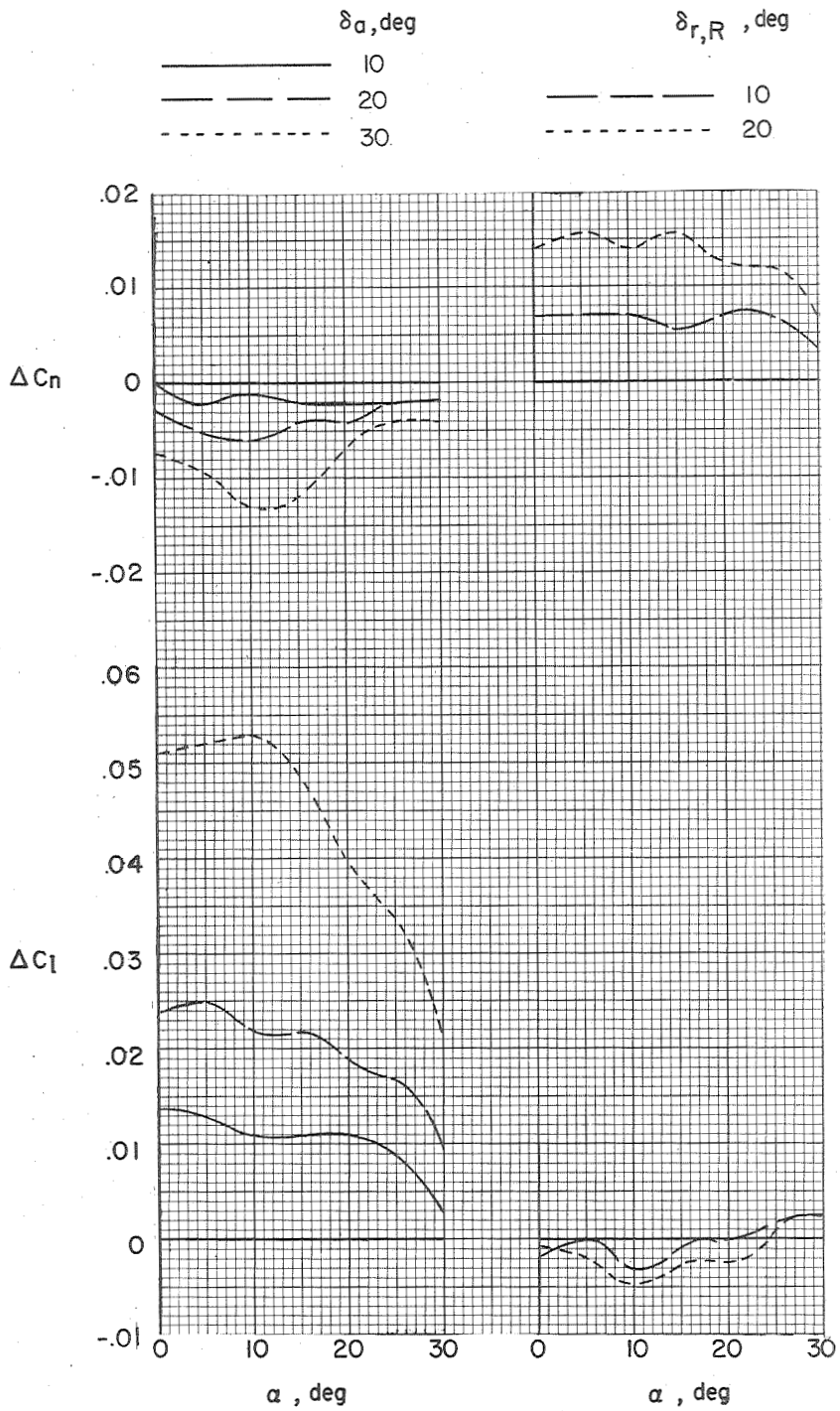

Figure 19.- Incremental rolling and yawing moments due to aileron and rudder control deflections. Model $B_3W_5V_5$.